J. Fluid Mech. (1998), *vol.* 357, *pp.* 321–349. Printed in the United Kingdom

Co-rotating stationary states and vertical alignment of geostrophic vortices with thin cores

By GEORGI G. SUTYRIN[1,2], JAMES C. McWILLIAMS[1,3] AND R. SARAVANAN[3]

[1] Institute of Geophysics and Planetary Physics, UCLA, Los Angeles, CA 90095, USA

[2] Graduate School of Oceanography, University of Rhode Island, Narragansett, RI 02882, USA

[3] National Center for Atmospheric Research, P.O. Box 3000, Boulder, CO 80307, USA

(Received 24 April 1996 and in revised form 15 August 1997)

We investigate the evolution of nearby like-sign vortices whose centres are at different vertical levels in a stably stratified rotating fluid. We employ two differently singularized representations of the potential vorticity distribution in the quasi-geostrophic equations (QG), in order to elucidate the pair-interaction behaviour previously seen in non-singular QG numerical solutions. The first is an analytically tractable conservative (Hamiltonian) elliptical-moment model (EM) for thin-core vortices, which exhibits a regime of very strong horizontal elongation of a vortex in response to the strain induced by its partner. We interpret this as an early evolutionary stage towards the irreversible dissipative merger and alignment interactions. This interpretation is strengthened by weakly dissipative numerical solutions of a thin-core contour-dynamics model (CD), which exhibit even further progress towards the completion of these vortex interactions in the same regime.

In the EM model we classify the co-rotating stationary states which exist always for vertically offset thin-core vortices. However, the mutual strain field among the vortices cannot be balanced by co-rotation in a weakly elongated stationary state for a certain class of neighbouring, but substantially non-aligned, vortex configurations, and our interpretive assumption is that such configurations will rapidly evolve in non-singular QG solutions towards a more aligned configuration through significantly non-conservative reorganizations of the potential vorticity field. Both the EM and CD models show qualitatively similar regime boundaries between evolutions with weakly and strongly deformed vortices. In particular, there is a fairly close correspondence between the occurrence of strong vortex elongation in the EM solutions and significant filamentation and splitting in the CD solutions.

1. Introduction

Large-scale atmospheric and oceanic motions are approximately geostrophic because of the influences of planetary rotation and stable density stratification. These flows often exhibit long-lived dynamically important patterns with a high degree of vertical correlation, often extending throughout the depth of the atmospheric troposphere or oceanic thermocline (if not the entire water column). Since the forcing of these motions is typically vertically more localized than their realized response, there must be evolutionary processes capable of establishing this correlation.

High-resolution numerical simulations show that, in both two- and three-

dimensional decaying geostrophic turbulence (2D and 3D QG), coherent vortices with spatially localized concentrations of potential vorticity emerge from an isotropic random initial state, and they eventually dominate the flow evolution (McWilliams 1984, 1989, 1990). The vortices move by mutual advection in an essentially conservative fashion except during close approaches when strongly dissipative interactions occur. The most important of these interactions occur between like-sign vortices: namely horizontal merger in 2D and 3D QG, where much of the core material of two vortices becomes entwined to form a single larger vortex, and vertical alignment in 3D QG of vortices centred at different vertical levels. With time, these processes reduce the vortex population, leading to fewer, larger, vertically grouped vortices. These vortex population tendencies are associated in both 2D and 3D QG with the approximate conservation of energy and its transfer to larger spatial scales (an inverse cascade), as well as the strong dissipation of potential vorticity variance (enstrophy) by its transfer to smaller scales (a forward cascade) – see Charney (1971).

Since merger occurs in the simpler two-dimensional case, it is at present better understood than alignment. Two-dimensional merger occurs when two vortices of the same sign and within a certain critical distance of each other mix a substantial portion of their core vorticity and become a single vortex (Melander, Zabusky & McWilliams 1988); this simple characterization is more apt for vortices of comparable strength since the interaction of quite disparate vortices leads to greater vorticity fragmentation in solutions of the contour-dynamics (CD) model (Dritschel & Waugh 1992; Dritschel 1995). Strong elongation of the vortex core in the initial stage of a merger results from the strong strain imposed by its nearby like-sign partner, and this elongation leads to vortex centres approaching each other in order to conserve angular momentum. Merger involves filamentation of the vorticity field and dissipation of the enstrophy, while preserving angular momentum about the vorticity centroid and the kinetic energy (at large Reynolds number). Two like-sign vortices separated by more than this critical distance remain separate and pulsate about a co-rotating stationary state. This co-rotating stationary state ceases to exist when the original separation distance is less than the critical value predicted well by a truncated elliptical-moment model (EM) for vortex movement and elongation (Melander, Zabusky & Styczek 1986; 1988; Abrashkin 1987). The absence of a co-rotating stationary state for small separation distances is connected with an unbounded elongation in time of the vortex core in a strong enough strain (e.g. Kida 1981). Thus, the merger condition in two dimensions is intimately connected with the non-existence of a non-axisymmetric stable co-rotating stationary state close to the initial configuration. Merger is the principal means of evolution of the population of coherent vortices in decaying two-dimensional turbulence, and the ultimate outcome of all possible mergers is a non-turbulent end-state of either a single monopole or a vortex dipole pair, depending upon whether the the total circulation is non-zero or not (Carnevale *et al.* 1992).

An early demonstration of alignment was made for the free evolution at modest Reynolds number in a two-layer QG model. From random initial conditions, a strong correlation developed between flow in the two layers, and the late time evolution was almost entirely barotropic (i.e. aligned) and on scales large compared to the internal deformation radius (Rhines 1977). This was interpreted as a consequence of the dual conservation of energy and potential enstrophy within wavenumber triads by Salmon (1982). Subsequent numerical solutions of fully three-dimensional decaying geostrophic turbulence at larger Reynolds number demonstrated the emergence of sparsely distributed coherent vortices (McWilliams 1989, 1990; McWilliams, Weiss & Yavneh 1994). These vortices emerge by a dual self-organization processes of

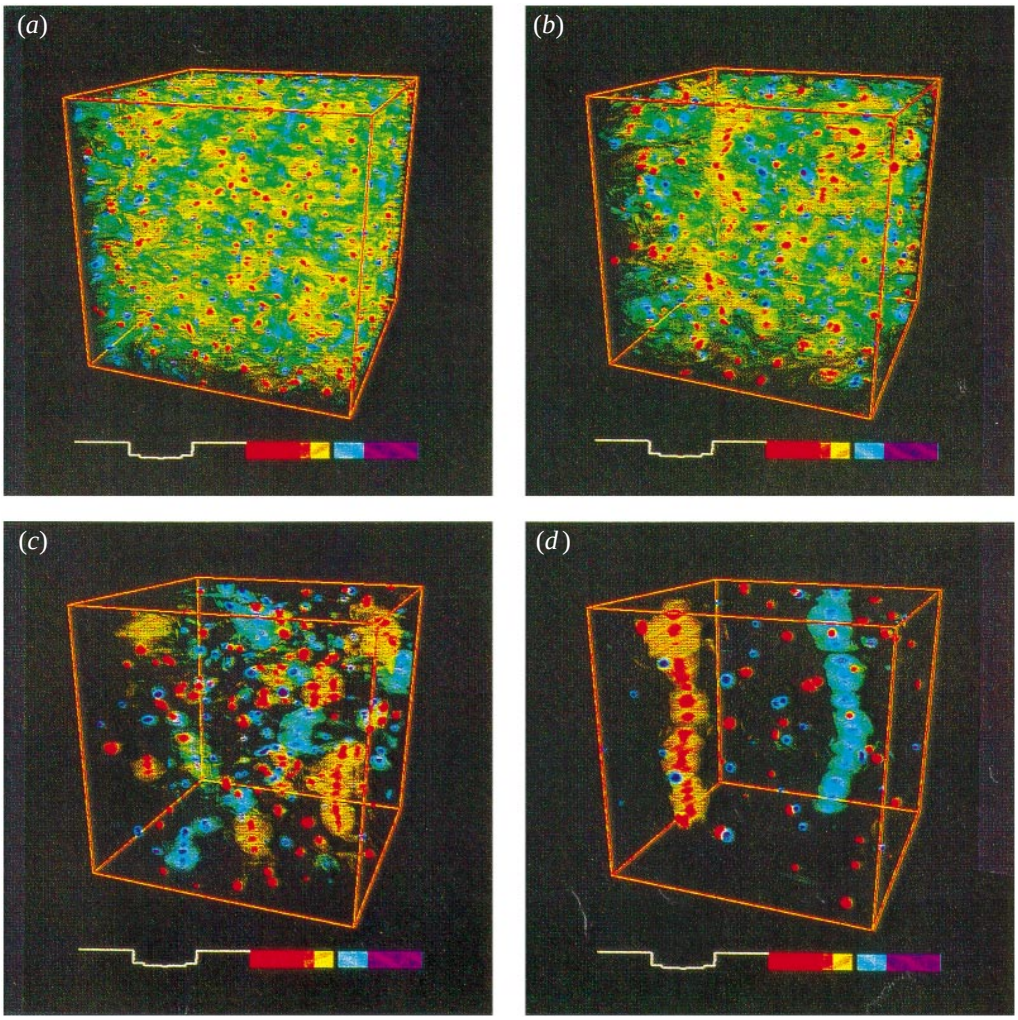

FIGURE 1. Potential vorticity field $q(x, y, z)$ at successive times in decaying geostrophic turbulence (from McWilliams *et al.* 1994).

horizontal axisymmetrization and vertical alignment, with correlation lengths whose aspect ratio H/L is roughly equal to f/N. A long-standing prediction of statistical theories is that geostrophic turbulence evolves to be spatially isotropic with this aspect ratio (Charney 1971; Rhines 1979; Herring 1980). More precisely, though, the mean H/L in numerical solutions is somewhat less than f/N after the vortices have developed, at least on the vortex-dominated scales smaller than the most energetic one.

With further evolution, however, separate vortices interact strongly when they make close approaches to each other during their chaotic motions (as occurs even in a point-vortex model), and one of the important outcomes is for the horizontal separation between the centres of like-sign vortices at different levels to diminish on average. An effect of this is for motions on spatial scales at least as large as the most energetic one to develop large vertical correlation lengths (i.e. to become more nearly equivalent-barotropic). The eventual outcome of this, after very many close

vortex interactions, is a non-turbulent stationary state of two well-separated columns of aligned axisymmetric same-sign vortices. Stages in this evolutionary sequence are illustrated in figure 1. Thus, alignment enters into the dynamics of coherent vortices in several stages: the initial self-organization of an individual vortex; recovery from tilting deformations induced by vertical shear (in close approaches); and evolution towards the horizontal coincidence of vortices at separate levels.

A few studies have already been made of alignment of isolated geostrophic vortices. The simplest baroclinic system is a two-layer QG CD model, with two patches of potential vorticity located in the different layers. The behaviour of a given initial configuration of potential vorticity has been shown to depend on its proximity to a doubly connected co-rotating stationary state (Polvani 1991). The novelty of alignment with respect to a merger is that in a two-layer fluid, the co-rotating stationary state exists also for small horizontal separation of vortices in different layers with a large amount of vertical overlap, which is impossible for vortices in the same layer. If an initial configuration is far from any stationary state, it has to rearrange itself considerably (through repeated filamentation) before it can approach a stationary state. Hence the occurrence of both merger and alignment, which are essentially inviscid processes in the early stages, depends on whether the vortex pair configuration is close to a stationary state; if not, then the vorticity often rearranges itself to the 'closest' available stationary state through an ultimately dissipative evolution. The recent development of the CD algorithm for three-dimensional QG has been used to demonstrate the importance of filamentation, hence enstrophy dissipation, in the evolution of an individual vortex with an initial potential vorticity distribution that is vertically tilted (Dritschel & Saravanan 1994; Viera 1995).

The simplest singularized model for 3D QG is point vortices with infinitesimal core size with movement by mutual advection among the vortices without any effects of core deformation (Gryanik 1983); since no tendency is found for alignment in this model, core deformations can be inferred to be important. The evolution of a three-dimensional QG vortex with a finite-size ellipsoidal vortex of uniform potential vorticity in a horizontally and vertically sheared external flow has been analysed by Zhmur & Pankratov (1989), Zhmur & Shchepetkin (1991), and Meacham *et al.* (1994). Using this approach for investigating the interaction of a vortex pair, Zhmur & Shchepetkin (1992) have shown a tendency for the ellipsoidal vortices to come together and collapse if the initial distance between them is smaller than a critical value. However, they considered only vortices at the same vertical level and thus demonstrated a tendency towards merger in a manner similar to two-dimensional QG.

As a next step toward understanding the interaction of vertically offset vortices, we consider the dynamics of vortices with an infinitesimal vertical thickness of the core region of uniform potential vorticity. This is an intermediate singularization between the point-vortex model and the ellipsoidal model of a vortex core with finite thickness; it takes into account only horizontal deformations of the vortex. However, when the vertical separation between thin vortices is small, their interaction may describe also the evolution of the shape of an individual vertically tilted vortex. The assumption of a thin core is consistent with the observed structure of some oceanic eddies, e.g. it reproduces the position of maximum angular velocity at the core boundary of young warm-core rings (Sutyrin 1989).

To analyse the interaction of vertically offset vortices with thin cores, we develop a perturbation approach assuming that the vortex centres are remote from each other compared to the size of an individual vortex. The interaction of vortices is

described in terms of the centroid motion, the horizontal elliptical deformation, and the rotation of the axis of the elliptical vortex in a manner similar to the EM model in 2D (Melander *et al.* 1986). This problem has a Hamiltonian formulation, as previously shown, in particular, for vortices with an ellipsoidal core by Zhmur & Pankratov (1990). As a partial assessment of the validity of this three-dimensional EM model, we compare its solutions with those of the less severely singularized three-dimensional QG CD model (Dritschel & Saravanan 1994), which permits the general deformation of vortex core boundaries, including their filamentation and fragmentation.

In § 2 we formulate the problem of vortex interactions in a rotating stratified fluid in terms of the centroid and local moments for every vortex with a compact core of uniform potential vorticity. In § 3 we consider the three-dimensional EM model for two equal vertically-offset thin-core vortices (with details of the derivation in the Appendix). In § 4, we analyse their stationary solutions, and in § 5 we analyse their integrable non-stationary dynamics. In § 6 we compare the solutions of the EM model with 3D CD numerical solutions for two identical thin-core vortices. Finally, in § 7 we summarize our findings and discuss the implications for non-singular potential vorticity distributions.

2. A moment expansion for vortices with compact cores of uniform potential vorticity

We start from the equation describing material conservation of QG potential vorticity on horizontal fluid trajectories,

$$\frac{\mathrm{D}q}{\mathrm{D}t} = \frac{\partial q}{\partial t} + u\frac{\partial q}{\partial x} + v\frac{\partial q}{\partial x} = 0. \tag{1}$$

For a uniformly rotating (i.e. f-plane), continuously stratified fluid, the non-dimensional QG relations for the dynamic pressure, p, the geostrophic velocity, $\boldsymbol{u} = (u, v)$, and the potential vorticity, q, are

$$u = -\frac{\partial p}{\partial y}, \quad v = \frac{\partial p}{\partial x}, \tag{2}$$

$$q = \nabla^2 p + \frac{\partial}{\partial z}\left(\frac{1}{N^2}\frac{\partial p}{\partial z}\right). \tag{3}$$

Here we use local Cartesian coordinates, (x, y, z), where z is the vertical coordinate in the direction of gravity and the axis of rotation. The underlying non-dimensionalization is by the horizontal scale, L, velocity scale, U, time scale, L/U, and vertical scale, $H = Lf/N_o$, where f is the Coriolis frequency, and N_o is the characteristic Brunt–Väisälä frequency (hence, $N^2(z)$ is the non-dimensional vertical gradient of the mean density profile).

By solving (3), the dynamic pressure can be expressed in terms of the Green's function $G(\rho, z, z')$, $2\rho = (x - x')^2 + (y - y')^2$, of the boundary-value problem for this three-dimensional elliptic operator:

$$p(x, y, z, t) = \overline{P}(x, y, z) + \int G(\rho, z, z')q(x', y', z')\mathrm{d}x'\mathrm{d}y'\mathrm{d}z'. \tag{4}$$

Here $\overline{P}$ is a the pressure field associated with a geostrophic stationary flow with uniform potential vorticity (i.e. a non-vortex background component).

We consider M vortices with compact cores of uniform potential vorticity q_k and define the centroid for each vortex by

$$\begin{pmatrix} X_k \\ Y_k \\ Z_k \end{pmatrix} = \frac{1}{W_k} \int_{W_k} \begin{pmatrix} x \\ y \\ z \end{pmatrix} \mathrm{d}x\,\mathrm{d}y\,\mathrm{d}z, \tag{5}$$

where W_k is the volume of the kth vortex. The vertical position of the vortex, Z_k, is time independent within the QG approximation.

We introduce M local coordinate systems $(x'_k,\ y'_k,\ z'_k)$, relative to the horizontal position of the kth centroid. For every vortex we decompose the velocity field $\boldsymbol{u}$ into a near field $\boldsymbol{u}_k$ and a far field $\boldsymbol{U}_k$. The near field is generated only by the kth vortex and can be expressed from (2) and (4) in the form

$$\boldsymbol{u}_k(x,y,z,t) = \begin{pmatrix} u_k \\ v_k \end{pmatrix} = q_k \int_{W_k} \hat{G}(\rho, z, z') \begin{pmatrix} -y + y' \\ x - x' \end{pmatrix} \mathrm{d}x'\mathrm{d}y'\mathrm{d}z', \tag{6}$$

where

$$\hat{G}(\rho, z, z') = \frac{\partial G}{\partial \rho}. \tag{7}$$

We write the far field as the sum of the background flow and the velocity field induced by the remaining vortices,

$$\boldsymbol{U}_k(x,y,z,t) = \begin{pmatrix} -\partial_y \overline{P} \\ \partial_x \overline{P} \end{pmatrix} + \sum_{\alpha \neq k}^{M} Q_\alpha \boldsymbol{U}_{k\alpha}, \tag{8}$$

$$\boldsymbol{U}_{k\alpha} = \begin{pmatrix} U_{k\alpha} \\ V_{k\alpha} \end{pmatrix} = \frac{1}{W_\alpha} \int_{W_\alpha} \hat{G}(\rho_\alpha, z, z') \begin{pmatrix} -y + Y_\alpha + y' \\ x - X_\alpha - x' \end{pmatrix} \mathrm{d}x'\mathrm{d}y'\mathrm{d}z', \tag{9}$$

$$2\rho_\alpha = (x - X_\alpha - x')^2 + (y - Y_\alpha - y')^2, \quad Q_\alpha = q_\alpha W_\alpha. \tag{10}$$

The centroid motion is governed by the far field only,

$$\begin{pmatrix} \dot{X}_k \\ \dot{Y}_k \end{pmatrix} = \frac{1}{W_k} \int_{W_k} \boldsymbol{U}_k \mathrm{d}x'\mathrm{d}y'\mathrm{d}z', \tag{11}$$

whereas both the near- and far-field components cause deformation and rotation of the vortex.

Using an expansion of $\boldsymbol{U}_k$ about the local vortex position, $\boldsymbol{R}_k = (X_k, Y_k, Z_k)$, gives

$$(\dot{X}_k, \dot{Y}_k) = \sum_{n=0}^{\infty} \sum_{m=0}^{n} \sum_{l=0}^{m} \frac{J_k^{(l,m-l,n-m)}}{l!(m-l)!(n-m)!} \partial_x^l \partial_y^{(m-l)} \partial_z^{(n-m)} \boldsymbol{U}_k|_{\boldsymbol{R}_k}, \tag{12}$$

where $J_k^{(l,m,n)}$ are the local geometrical moments of the vortex core region, namely

$$J_k^{(l,m,n)} = \frac{1}{W_k} \int_{W_k} x'^l y'^m z'^n \mathrm{d}x'\mathrm{d}y'\mathrm{d}z' \tag{13}$$

with $x' = x - X_k$, etc. The evolution equations for the local geometrical moments are derived from (13) in the same manner as suggested by Melander *et al.* (1986) for the two-dimensional Euler equations

$$\dot{J}_k^{(l,m,n)} = \dot{J}_{*k}^{(l,m,n)} + \frac{1}{W_k} \int_{W_k} x'^{(l-1)} y'^{(m-1)} z'^n [mx'(V_k - \dot{Y}_k) + ly'(U_k - \dot{X}_k)] \mathrm{d}x'\mathrm{d}y'\mathrm{d}z', \tag{14}$$

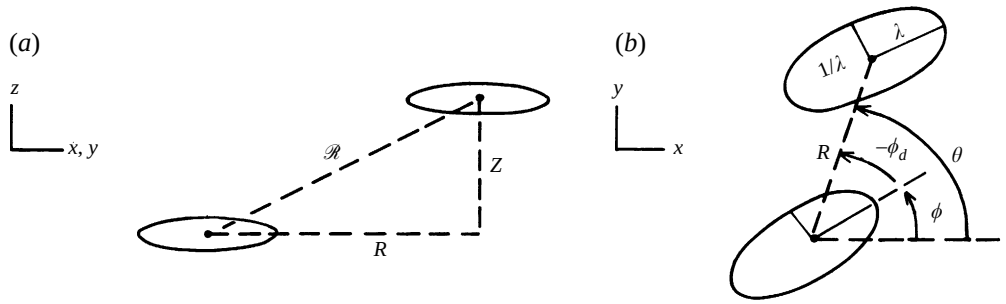

FIGURE 2. Schematic drawing of two thin elliptical vortices: (*a*) side view; (*b*) top view.

where the second term describes the influence of the far field and $\dot{J}_{*k}^{(l,m,n)}$ describes the vortex self-interaction,

$$\dot{J}_{*k}^{(l,m,n)} = \frac{1}{W_k}\int_{W_k} x'^{(l-1)}y'^{(m-1)}z'^{n}(mx'v_k + ly'u_k)\mathrm{d}x'\mathrm{d}y'\mathrm{d}z'. \tag{15}$$

The first local moments (e.g. $J^{(1,0,0)}$) are zero because of the definition of the centroids (5).

By using (6)–(9) with local expansions of $\boldsymbol{U}_k$ and $\boldsymbol{u}_k$ around $\boldsymbol{R}_k = (X_k, Y_k, Z_k)$, the integrals in (14) and (15) are expressed in terms of the local geometrical moments. Thus, (12)–(15) constitute an infinite system of ordinary differential equations.

For the remainder of this paper, for simplicity and analytical tractability, we consider only vortices with a thin core, assuming

$$\kappa_k \equiv \frac{W_k}{A_k^{3/2}} \ll 1, \tag{16}$$

where A_k is the area of the horizontal section of the vortex at its central level $z = Z_k$ (A_k is conserved in QG because the geostrophic horizontal velocities are non-divergent). In this case we may neglect the effects of moments (13) with $n \geqslant 1$ because they are proportional to κ_k^n.

The successive moments (14) can be shown to contribute to the far-field velocity proportional to successive powers of the ratio of the vortex core size to the vortex separation. Therefore, if we assume that all vortices are well separated, either horizontally or vertically, we truncate the evolution equations, (12) and (14), at their first non-trivial order to derive the second-order elliptic-moment model (EM) for thin-core vortices in three dimensions (see the Appendix).

3. Evolution equations for two equal vortices

Using the EM model, we consider the interaction of two equal vortices which are horizontally and vertically offset with centres at (X, Y, Z) and $(-X, -Y, 0)$, hence with a horizontal separation distance of $R = 2(X^2 + Y^2)^{1/2}$. Each vortex is characterized by its volume-integrated potential vorticity, Q, horizontal moment of inertia, J (see equation (A 7)), aspect ratio, λ (the square root of the ratio of major and minor axes of the elliptical deformation of the vortex core), and the angle ϕ between the major axis and x-direction (see figure 2).

From (A 25)–(A 27) the centroid motion is described by

$$\begin{pmatrix}\dot{X}\\ \dot{Y}\end{pmatrix} = Q\left\{R\hat{G} + \frac{\mu}{R}J\Upsilon\left[\lambda + \frac{1}{\lambda} + \left(\lambda - \frac{1}{\lambda}\right)\cos(2\phi - 2\theta)\right]\right\}\begin{pmatrix}-\sin\theta\\ \cos\theta\end{pmatrix} + \frac{2}{R}QJ\Upsilon\left(\lambda - \frac{1}{\lambda}\right)\begin{pmatrix}\sin(2\phi - 3\theta)\\ \cos(2\phi - 3\theta)\end{pmatrix}, \quad (17)$$

where the induced angular velocity $\hat{G}$, strain rate Υ and coefficient μ are defined by

$$\hat{G} = \frac{1}{4\pi(R^2 + Z^2)^{3/2}}, \quad \Upsilon = \frac{3R^2}{8\pi(R^2 + Z^2)^{5/2}}, \quad \mu = \frac{R^2 - 4Z^2}{R^2 + Z^2}. \quad (18)$$

Thus, for the evolution of R and $\theta = \tan^{-1}(Y/X)$ we obtain

$$\dot{R} = 2\dot{X}\cos\theta + 2\dot{Y}\sin\theta = \frac{4}{R}QJ\Upsilon\left(\lambda - \frac{1}{\lambda}\right)\sin(2\phi_d), \quad (19)$$

$$\dot{\theta} = \frac{2}{R}(\dot{Y}\cos\theta - \dot{X}\sin\theta) = 2Q\left\{\hat{G} + \frac{J\Upsilon}{R^2}\left[\mu\left(\lambda + \frac{1}{\lambda}\right) + (\mu + 2)\left(\lambda - \frac{1}{\lambda}\right)\cos(2\phi_d)\right]\right\}, \quad (20)$$

where the angle variables appear only in the combination $\phi_d \equiv \phi - \theta$, which is the angle between the major axis of the elliptical vortices and the line separating the vortex centres. For the orientation and aspect ratio, equations (A 39)–(A 40) give

$$\dot{\lambda} = -2\lambda Q\Upsilon\sin(2\phi_d), \quad (21)$$

$$\dot{\phi}_d = \dot{\phi}^{(i)} - \dot{\theta} + Q(\hat{G} - \Upsilon) - Q\Upsilon\frac{\lambda^2 + 1}{\lambda^2 - 1}\cos(2\phi_d). \quad (22)$$

Thus, the relative rotation rate $\dot{\phi}_d$ depends on the sum of influences among the self-rotation, $\dot{\phi}^{(i)}$, mutual rotation, $\dot{\theta}$, and the shear-induced rotation of one vortex by the far-field velocity of the other, which has a local rotation component $Q(\hat{G} - \Upsilon)$ and a strain component described by the last term in (22).

Conservation of angular momentum T (see (A 47)) in EM follows from the combination of (19) and (21), which provides an integral relation that allows the elimination of R:

$$R^2 + 4J\left(\lambda + \frac{1}{\lambda}\right) = \frac{2T}{Q}. \quad (23)$$

Conservation of energy (A 48) gives another integral which can be used for eliminating ϕ_d:

$$\frac{H}{Q^2} = \frac{2H^{(i)}}{Q^2} - G - J(\hat{G} - \Upsilon)\left(\lambda + \frac{1}{\lambda}\right) + J\Upsilon\left(\lambda - \frac{1}{\lambda}\right)\cos 2\phi_d = \text{const}. \quad (24)$$

Here the Green's function is $G = -1/4\pi(R^2 + Z^2)^{1/2}$, and the self-energy $H^{(i)}$ depends on λ only according to (A 57)–(A 58). Thereby, the system is reduced to an integrable equation for λ only, as for 2D vortices (Melander *et al.* 1988). The system (20)–(23) is autonomous; therefore, for a fixed value of the conserved quantities Z and T, the trajectories in the $(\lambda, 2\phi_d)$-plane are the level curves of H, (24).

We can simplify the equations above by an appropriate transformation based on $2J^{1/2}$ for distance, $Q^2/16\pi J^{1/2}$ for energy, $Q/16\pi J^{3/2}$ for rotation rate, and $2JQ$ for

angular momentum. Thus, the energy (24) becomes

$$h(\lambda, \phi_d; \sigma, Z) = h^{(i)} + \frac{2}{(R^2+Z^2)^{1/2}} + \frac{3}{4(R^2+Z^2)^{5/2}}\left[(R^2-2Z^2)\left(\lambda+\frac{1}{\lambda}\right) + R^2\left(\lambda-\frac{1}{\lambda}\right)\cos 2\phi_d\right], \quad (25)$$

where the self-energy is

$$h^{(i)} \equiv 32\pi\frac{J^{1/2}H^{(i)}}{Q^2} = \chi h_e, \quad (26)$$

and, by (A 57) and (A 67) for an ellipsoidal core,

$$\chi = 16\pi\frac{J_e^{3/2}\kappa_e}{W_e} = \frac{12}{5\sqrt{5}}. \quad (27)$$

The normalized self-rotation frequency is

$$\omega^{(i)} = \chi\omega_e(\lambda, 0), \quad (28)$$

where ω_e is defined by (A 42) for an elliptical vortex. We will keep the same notation for normalized distances R and Z; e.g. R^2 is expressed from (23) as

$$R^2 = \sigma^2 + 2 - v, \quad v \equiv \lambda + \frac{1}{\lambda}, \quad (29)$$

where $\sigma^2 + 2 = T/2QJ$ denotes the normalized angular momentum, i.e. $\sigma \equiv (T/2QJ - 2)^{1/2}$, so that $R = \sigma$ for circular vortices with $\lambda = 1$.

4. Stationary states

Stationary solutions are found only for $\phi_d = 0$ (see (21)), where the separate rotational influences in (22) balance in a configuration where the major axes are parallel to the centre separation line. This corresponds to extrema of h, i.e. to zeros of the slope $\mathrm{d}h/\mathrm{d}\lambda$ along the direction $\phi_d = 0$,

$$\frac{\mathrm{d}h}{\mathrm{d}\lambda} = \gamma + \left(1 - \frac{1}{\lambda^2}\right)[\omega\prime - \omega^{(i)}] = 0, \quad (30)$$

where

$$\gamma = \frac{3(\sigma^2+2-v)}{2(\sigma^2+2-v+Z^2)^{5/2}} \quad (31)$$

is the normalized strain rate and

$$\omega' = \frac{1}{2(\sigma^2+2-v+Z^2)^{3/2}} + \frac{3(\mu+1)\lambda^2-3}{4\lambda(\sigma^2+2-v+Z^2)^{5/2}} \quad (32)$$

is the correction to rotational frequency due to mutual and local rotation. The solutions of (30) are defined in the interval $1 < \lambda < \lambda_{max}(\sigma)$, where

$$\lambda_{max} = [2 + \sigma^2 + \sigma(\sigma^2+4)^{1/2}]/2 \quad (33)$$

corresponds to zero horizontal separation.

When $\lambda = 1$, this slope is always positive,

$$\frac{\mathrm{d}h}{\mathrm{d}\lambda} = \gamma = \frac{3\sigma^2}{2(\sigma^2+Z^2)^{5/2}} > 0, \quad (34)$$

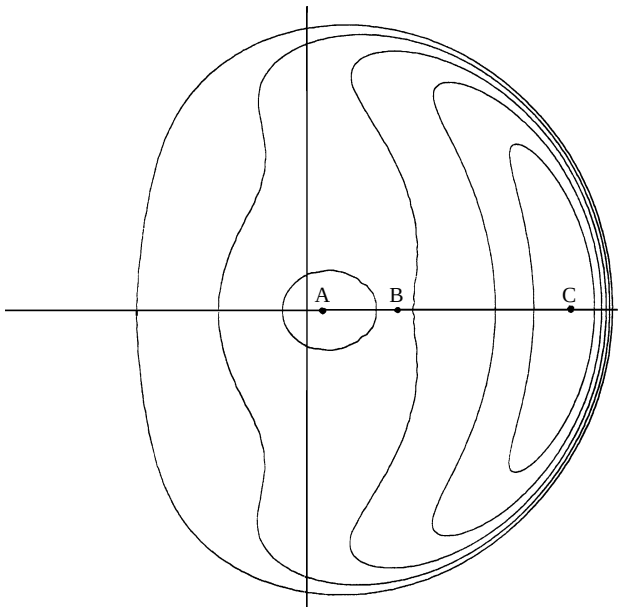

FIGURE 3. Isolines of energy, h, plotted using polar coordinates $(\lambda - 1, 2\phi_d)$ for two identical thin elliptical vortices (when $Z = 1$ and $\sigma = 2.8$). These are also phase-plane trajectories. Stationary states A and C are local maxima and B is a saddle point.

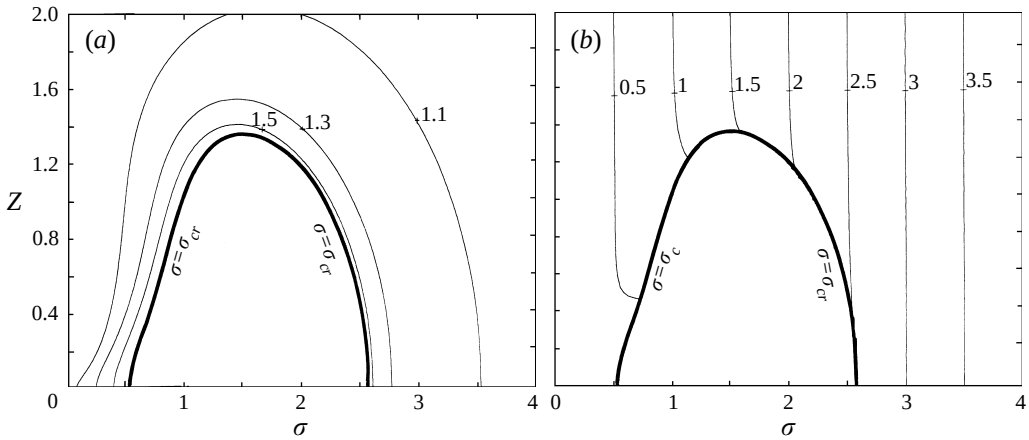

FIGURE 4. Stationary state A: (*a*) aspect ratio $\lambda(\sigma, Z)$ and (*b*) horizontal separation $R(\sigma, Z)$. The bold line is $\lambda = 1.7$, which represents the regime boundaries $\sigma_C(Z)$ when $\sigma < 1.7$ and $\sigma_{cr}(Z)$ when $\sigma > 1.7$.

while for $\lambda \to \lambda_{max}(\sigma)$ the slope (30) becomes infinite only for vortices at the same vertical level ($Z = 0$ and $\mu = 1$) because $\gamma \to \infty$. In this particular case, (30) has two solutions, $\lambda = \lambda_A(\sigma)$ and $\lambda = \lambda_B(\sigma) > \lambda_A$ when $\sigma > \sigma_{cr}$ as for two dimensions. These solutions merge: $\lambda_A = \lambda_B$ at $\sigma = \sigma_{cr}$. The critical value here is $\sigma_{cr} \approx 2.7$ at $\lambda \approx 1.7$; both σ_{cr} and the corresponding horizontal distance $R \approx \sigma_{cr}$ are less in the three-dimensional EM model than in the two-dimensional EM model where $\sigma_{cr} \approx 3.3$.

The situation is different for vertically offset vortices with $Z > 0$. From (31)–(32)

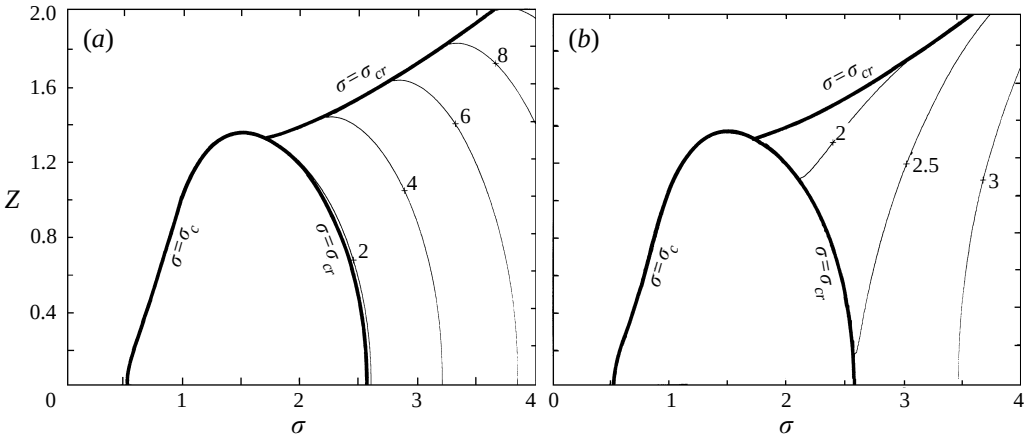

FIGURE 5. Same as figure 4, but for stationary state B. The upper part of the regime boundary σ_{cr} for $Z > Z_{cr}$ is also shown as the bold line.

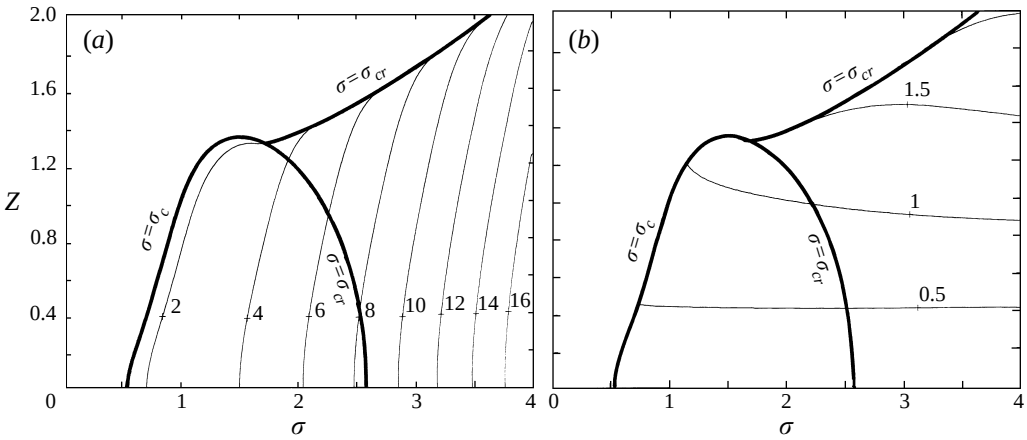

FIGURE 6. Same as figure 5, but for stationary state C.

and (18), we see that $\gamma \to 0$ and $\mu \to -4$ when $\lambda \to \lambda_{max}$, while

$$\omega' \to \frac{1}{2Z^3} - \frac{3(3\lambda^2+1)}{4\lambda Z^5}. \tag{35}$$

For any fixed $\lambda_{max}(\sigma)$, the maximum value of ω' is achieved for $Z^2 = (15\lambda_{max}^2+5)/2\lambda_{max}$, so that

$$\omega^{(i)}(\lambda_{max}) > \omega' \tag{36}$$

for the normalized internal frequency (28). Therefore, the slope is negative in (30). The change of the sign of the slope for any $Z > 0$ proves that at least one stationary state always exists for vertically offset vortices.

There is only one stationary state if $\sigma < \sigma_{cr}(Z)$, while there are three stationary states when $\sigma > \sigma_{cr}(Z)$. Besides the centre A and a saddle point B (which also exists for two-dimensional vortices), there also exists another centre C with large aspect ratio $\lambda_C > \lambda_B > \lambda_A$ (figures 3–6). $\sigma_{cr}(Z)$ has two branches. The states A and B merge

at the boundary $\sigma = \sigma_{cr}(Z)$, $Z \leqslant Z_{cr}$, while the states B and C merge at the boundary $\sigma = \sigma_{cr}(Z)$, $Z \geqslant Z_{cr}$. All three of them merge at $\sigma = \sigma_{cr}(Z_{cr}) \approx 1.7$, $Z = Z_{cr} \approx 1.3$.

The centre C, characterized by large horizontal aspect ratio ($\lambda_C > 1.7$), exists when $\sigma > \sigma_C(Z)$ (figure 6). The critical value is either $\sigma_C(Z) = \sigma_{cr}(Z)$, for $Z > Z_{cr}$, or $\sigma_C(Z) < \sigma_{cr}(Z)$, for $Z < Z_{cr}$. The aspect ratio in state C, λ_C, increases when the vertical separation Z decreases with fixed σ and when σ increases with fixed Z. When $Z \ll \sigma$, the vortices are strongly elongated: $\lambda_C \approx \sigma^2$ for large σ (figure 6).

On the other hand, when $\sigma < \sigma_C(Z)$, the only stationary state is A, and it has a moderate aspect ratio $\lambda_A < 1.7$ for both remote and nearly aligned vortices (figure 4). This is because for $Z > 0$ the strain rate decreases when $R \to 0$, and $\lambda \to 1$, unlike for two-dimensional vortices. Indeed, when $\sigma \ll Z$, we can show from (30) and (36) that

$$\lambda_A^2 - 1 \approx \frac{3\sigma^2}{2Z^5\omega_0^{(i)} - Z^2 + 6} \ll 1, \tag{37}$$

where $\omega_0^{(i)} \equiv \chi\omega_e(1,0) \approx 0.2$ is the internal rotational frequency of a thin circular vortex.

As seen in figures 4–6, for any $\lambda > 1$ the stationary solution $\sigma(Z,\lambda)$ has an arch shape in (σ, Z) with two branches. At the outer branch with larger σ, the strain rate γ in (30) is mainly balanced by the self-rotation $\omega^{(i)}$, while at inner branch with smaller σ, the strain rate is mainly balanced by mutual and local rotation ω'. Both $\omega^{(i)}$ and ω' are important to balance the strain rate at the upper part of the arch. For moderate $\lambda < 1.7$, both branches belong to stationary state A (figure 4), while for $\lambda > 1.7$ the outer branch belongs to the unstable state B (figure 5) and the inner branch belongs to the state C (figure 6).

The most important result of this analysis is the non-existence of state A with moderate aspect ratio when $\sigma_C(Z) < \sigma < \sigma_{cr}(Z)$ and $Z < Z_{cr}$ (figure 4). Only a state C with large aspect ratio exists in this regime.

5. Transient evolution

The problem of two identical vortices in the EM model with given vertical separation Z and angular momentum $\sigma^2 + 2$ is an integrable Hamiltonian dynamics with a single degree of freedom. Thus, we can describe the general transient evolution in movement along the isolines of h as a function of the polar coordinates $(\lambda - 1,\ 2\phi_d)$; thus, these isolines are also the phase-space trajectories (figure 3). The origin in this plane represents a circular vortex ($\lambda = 1$). As we move away from the origin, λ increases and R decreases in order to preserve angular momentum. The horizontal separation reaches zero on a circle of radius $\lambda = \lambda_{max}$. Figure 3 is reflection symmetric between top and bottom, corresponding to the time-reversibility of the system (21)–(22).

For vortices at the same vertical level ($Z = 0$), the structure of h in three dimensions is similar to the two-dimensional case analysed by Melander *et al.* (1988). As mentioned in §4, a pair of stable and unstable stationary solutions exist for remote vortices when $\sigma > \sigma_{cr}$. The stable state corresponds to a centre A and non-stable state corresponds to a saddle point B with larger aspect ratio $\lambda_B > \lambda_A$. Inside the separatrix, starting and ending at saddle point B, there are closed orbits around the centre A, describing co-rotating pulsating vortices. All orbits outside this separatrix are open and lead to centroid collapse at the point $(\lambda = \lambda_{max}, \phi_d = -\pi/4)$, which has been interpreted as the irreversible tendency towards merger for sufficiently close

vortices in non-singular solutions. The minimum value $\sigma = \sigma_{cr}$ corresponds to one unstable stationary state, and for $\sigma < \sigma_{cr}$ all trajectories end at the point of collapse.

There is no collapse for vertically offset vortices ($Z > 0$) because at least one stationary state always exists and all orbits are closed. Along an orbit not surrounding the origin, ϕ_d oscillates around zero, corresponding to a nutation of elliptical vortices in the co-rotating frame. On orbits surrounding the origin, ϕ_d increases steadily, so that vortices rotate in the co-rotating frame.

Although elliptical vortices can have arbitrarily large $\lambda(t)$, such highly deformed shapes are unlikely to be stable in non-singular QG dynamics, where the non-conservative behaviours of filamentation and fragmentation of vortices are likely. Thus, we interpret large λ values as likely situations for significant potential vorticity dissipation and reconnection behaviours outside the EM model in non-singular QG dynamics, possibly indicating an irreversible tendency towards alignment. This, of course, must be confirmed (see § 6).

Consider the h phase plane for the three regimes discussed in § 4:

(*a*) $\sigma > \sigma_{cr}(Z)$. This is most complicated and interesting case. Besides the centre C, we have a pair of stable and unstable stationary states which correspond to the previously considered centre A and saddle point B that exist for vortices at the same level; therefore, $\lambda_A < \lambda_B < \lambda_C$ (figure 3). Inside the separatrix, starting and ending at saddle point B, and surrounding the centre A with moderate aspect ratio, all orbits are closed around the centre A, so that $\lambda < \lambda_B$. Outside this separatrix, all orbits are closed around either both centres A and C or only centre C with large λ. Instead of tending to the collapse point as for vortices at the same level, all trajectories intersect the $\phi_d = 0$ line with $\lambda > \lambda_C$. Here the horizontal distance between vortices decreases to a small value while they become strongly elongated: $\lambda_C \approx \sigma^2 \gg 1$ when $Z \ll \sigma$ (as mentioned above).

To characterize the conditions that distinguish whether λ must become large, we focus on the critical separatrix determined by the value of h (27) at the saddle point B, namely

$$h_B(\sigma, Z) = h(\lambda_B, 0; \sigma, Z), \tag{38}$$

where $\lambda_B(\sigma, Z)$ denotes the aspect ratio of state B. The region of the phase plane inside the separatrix is then described by

$$h(\lambda, 2\phi_d; \sigma, Z) > h_B(\sigma, Z), \quad \lambda < \lambda_B(\sigma, Z). \tag{39}$$

Hence, when $\sigma > \sigma_{cr}(Z)$, strong deformation will occur if and only if either of the following conditions is satisfied:

$$h < h_B(\sigma, Z) \quad \text{or} \quad \lambda > \lambda_B(\sigma, Z). \tag{40}$$

This deformation condition is similar to the merger condition in two dimensions (i.e. (31) in Melander *et al.* 1988) except when $\sigma < \sigma_{cr}$.

(*b*) $\sigma_C(Z) < \sigma < \sigma_{cr}(Z)$ and $Z < Z_{cr}$. All orbits are closed around the only stationary state C, and the solutions reach a large λ value ($> \lambda_C$) on their orbit (see figure 6 *a*).

(*c*) $\sigma < \sigma_C(Z)$. All orbits are closed around the stationary state A with moderate aspect ratio. Starting from circular vortices, λ may only slightly exceed 2 (figure 4 *a*).

An overview of this deformation behaviour is given in figure 7, which shows the maximum aspect ratio along an orbit for initially circular vortices with separation distances (R, Z). We see that large deformations occur only in a region of finite Z and intermediate R, which is close to the region where state A does not exist (figure

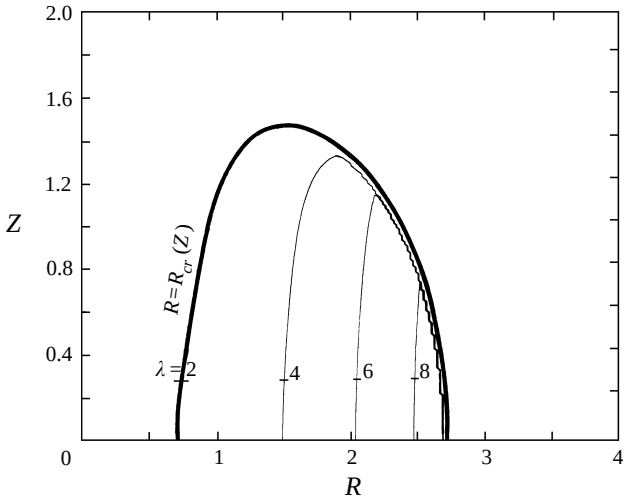

FIGURE 7. Maximum of the horizontal aspect ratio over the oscillation period for initially circular vortices, as a function of initial separation distances, R and Z. The line $R = R_{cr}(Z)$ is defined by the criterion $\max_t[\lambda] = 2$.

4 *a*). We define a double-valued curve $R = R_{cr}(Z)$ which separates solutions with weak deformation from those with strong deformation, by the criterion $\max_t[\lambda] = 2$.

6. Contour dynamics of thin vortices

In this section we examine the reliability of the EM model by comparison with CD solutions of the QG equations (1)–(3), while retaining the assumption of thinness, $\kappa \ll 1$. We use a multi-layer numerical model of CD (Dritschel & Saravanan, 1994) with $N(z) = 1$ and total fluid depth $D = 4$ (which we have confirmed is large enough compared to Z so that the effects of the rigid boundary conditions at the surface and bottom in the model are small). Initially the vortices each have a circular core of uniform potential vorticity with radius $r_c = 1$ in two vertically separated layers. Thus, if the total number of layers is n and a vortex core occupies one of n layers, the core thickness is $\kappa = D/n \ll 1$. The calculations were done with both $n = 25$ and $n = 51$ to confirm the insensitivity to the particular value of κ, provided that it is small.

Figure 8 is a comparison of the regime boundaries, $R = R_{cr}(Z)$, for EM and CD solutions. The deformation criterion required for CD is a more general one of vortex boundary stretching and filamentation than in the EM model where $\lambda(t)$ is the only available measure; for CD the appropriate measure is the vortex boundary length $S(t)$ (normalized such that $S(0) = 1$ for the circle). There is, of course, some arbitrariness in choosing the threshold values for these deformation measures, and we need not expect that their correspondences be close in all circumstances. Nevertheless, in both models there are transitions between weakly and strongly deformed transient solutions near the curves associated with the stationary-state transitions, σ_C and σ_{cr} for $Z < Z_{cr}$. However, the closeness of their correspondence varies along the transition boundary, so we will consider in turn each of the outer, inner, and upper boundary segments.

6.1. *Outer boundary*

First, we consider the outer boundary segment of $R = R_{cr}(Z)$, demarcated on figure 8 as pairs of CD solutions spanning the boundary at $Z = 0.64$, 0.32, and 0. These pairs

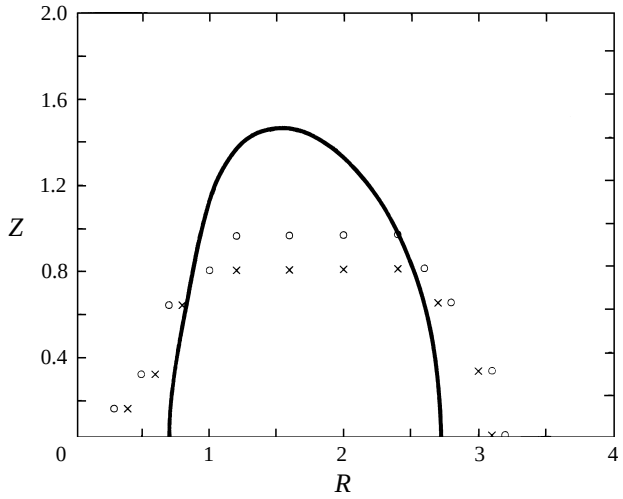

FIGURE 8. Regime boundaries between weakly and strongly deformed shapes in their subsequent evolution for initially circular vortices, as a function of initial separation distances, R and Z. The solid line is the line $\max_t[\lambda] = 2$ for thin elliptical vortices (from figure 7), and the circles and crosses indicate CD solutions with $\max_t[S] <$ and > 1.2, respectively.

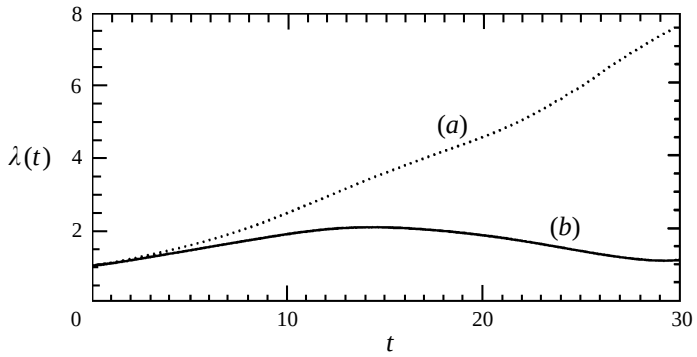

FIGURE 9. $\lambda(t)$ in CD for two of the initial (R, Z) values shown in figure 8: (*a*) (2.60, 0.64); (*b*) (2.80, 0.64).

show strong differences in $\lambda(t)$ for close initial conditions near R_{cr} (figure 9), as well as in the $S(t)$ criterion that we have used to identify the boundary. For this segment the boundary is at somewhat larger R for CD solutions than for EM solutions, and this difference increases as Z decreases; however, the general shape of the boundary is similar in the two models. When the shape deformations are strong (i.e. in the solutions marked with a cross), the aspect ratio dramatically increases with time, while the horizontal separation for at least some parts of the vortex cores decreases, indicating a tendency towards amalgamation of the potential vorticity originally in the vortex cores. For solutions with smaller deformations (i.e. marked by a circle), the vortex pairs co-rotate with pulsating aspect ratio $\lambda < 2.5$; this corresponds to a phase-plane trajectory around the stationary state A.

For $Z = 0.64$ and $R < R_{cr}$, after a strong early elongation, the vortex cores split into two pairs, with only a modest amount of accompanying potential-vorticity filamentation (figure 10 *a*). The inner members of each pair move into a configuration

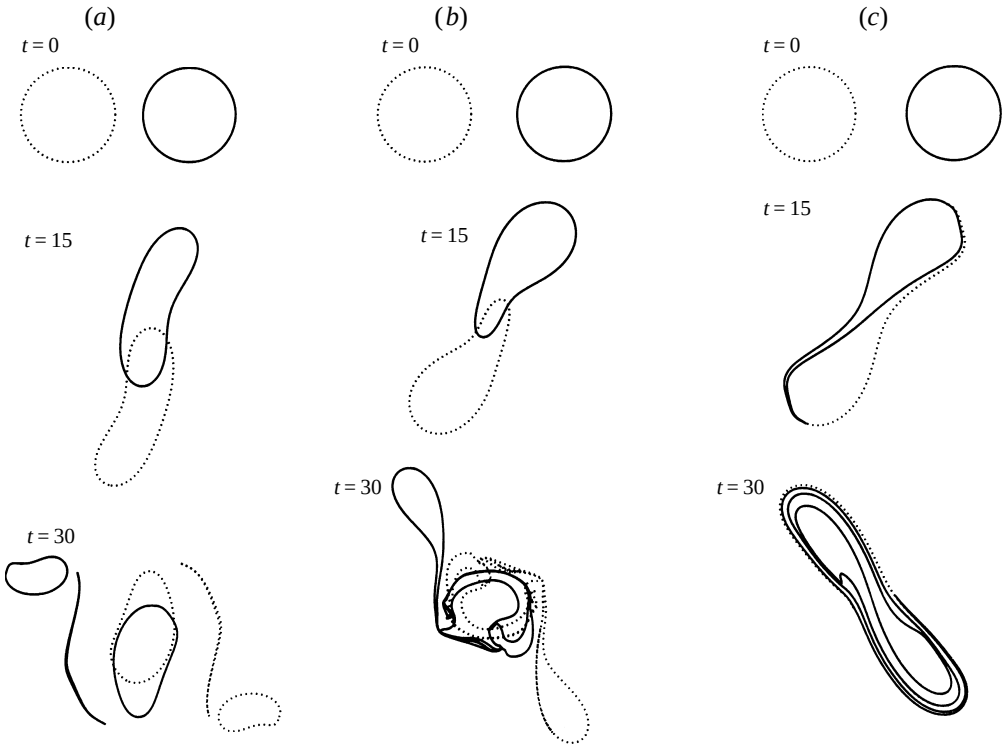

FIGURE 10. A horizontal projection of the vortex shapes in CD solutions near the outer regime boundary for (*a*) $(R, Z) = (2.60, 0.64)$; (*b*) $(R, Z) = (3.00, 0.32)$; (*c*) $(R, Z) = (3.10, 0.00)$.

of near alignment, while the outer members move outward and continue to co-rotate as remote vortices. For $Z = 0.32$, strong core deformations again lead to splitting of the vortices into two pairs, with both larger and smaller horizontal separations than initially (figure 10*b*). The inner pair is very strongly deformed here; although there is a suggestion of some tendency towards reformation as a nearly aligned vortex, this type of 'reconnection' process is difficult to follow very far towards completion in a CD solution. For vortices centred at the same level ($Z = 0$), there is a tendency towards amalgamation by winding themselves around each other, as in two-dimensional merger (figure 10*c*). In all of these CD examples for $R < R_{cr}$, there is strong evidence in support of non-conservative effects through 'instability' of the large elliptical deformations that arise in the EM solutions, as well as a subsequent evolution towards amalgamation, i.e. alignment and/or merger.

6.2. *Inner boundary*

For vertically separated vortices near the inner boundary R_{cr}, we have calculated pairs of CD solutions at $Z = 0.64$, 0.32, and 0.16 in figure 8 (we avoid $Z \to 0$ since the approximation of thin vortex cores is not meaningful there). Here the boundary for CD solutions lies at somewhat smaller R than for EM solutions, but again it has a roughly similar shape. The CD solutions for $R > R_{cr}$ do not develop large λ values, in contrast to the behaviour near the outer boundary (figure 10). Rather they exhibit a strong growth of boundary length $S(t)$ leading to filamentation but with all the detached fragments remaining close to the original range of horizontal separation

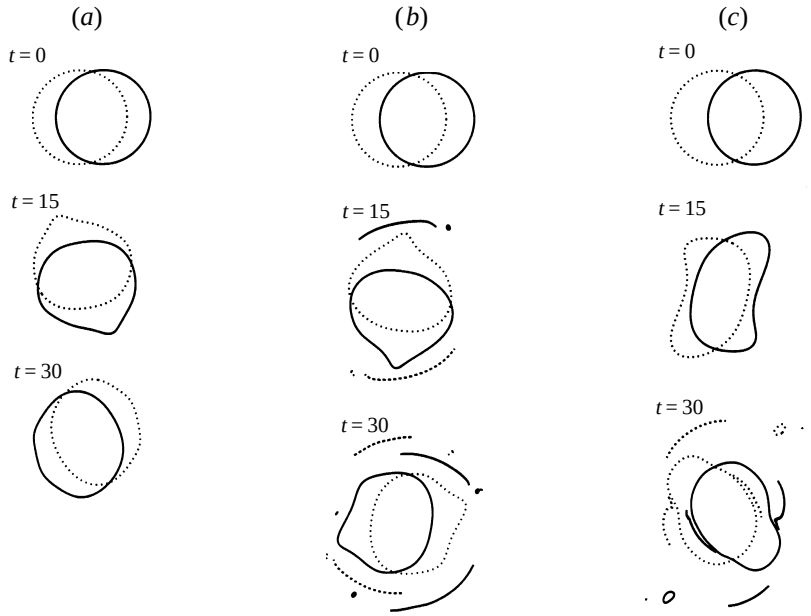

FIGURE 11. A horizontal projection of vortex shapes in CD solutions near the inner regime boundary for (*a*) $(R, Z) = (0.50, 0.32)$; (*b*) $(R, Z) = (0.60, 0.32)$; (*c*) $(R, Z) = (0.80, 0.64)$.

distances. The greater part of the vortex core remains fairly close to a circular shape, with local bulges or kinks developing as the filamentation sites.

For $Z = 0.32$ and $R < R_{cr}$, the bulge does not proceed to filamentation and instead evolves as a dispersive wave along the vortex boundary (figure 11 *a*). For the same Z and $R > R_{cr}$, the bulges develop into kinks and filaments that move outward horizontally, and the horizontal distance between the surviving vortex cores decreases somewhat, indicating a progression towards greater alignment (figure 11 *b*). For $Z = 0.64$ and $R > R_{cr}$, there is greater growth in λ, more filamentation, the appearance of a pair of small vortices at large R, and a somewhat greater decrease in R between the primary vortex cores (figure 11 *c*). Overall, the amount of deformation, non-conservation of core vorticity, and relative change in R are less near the inner boundary than near the outer one, since the vortices start less far from an aligned configuration.

6.3. *Upper boundary*

Finally we consider pairs of initially circular vortices at $Z = 0.8$ and 0.96 for several R values (figure 8). These pairs again straddle the boundary between weakly and strongly deformed vortex evolutions. This portion of the boundary lies at significantly smaller Z than for EM solutions. Part of this difference in boundary locations is due to the difference in the defining criterion for the boundary: the 'stable' CD solutions here (the circles along the upper boundary) are able to sustain $\lambda > 2$ without excessive growth in boundary length nor any filamentation, which is an indication that our two threshold criteria involving λ and S are not universally compatible. Nevertheless, a CD solution $R = 1.6$ and $Z = 1.28$ has $\max_t [\lambda(t)]) = 1.5$, and thus it lies within the weakly deformed regime well below the $Z \approx 1.4$ for the EM model.

This difference between the EM prediction and CD also can be partly understood by analysing the stationary solutions of (22). From (30), these solutions can be written

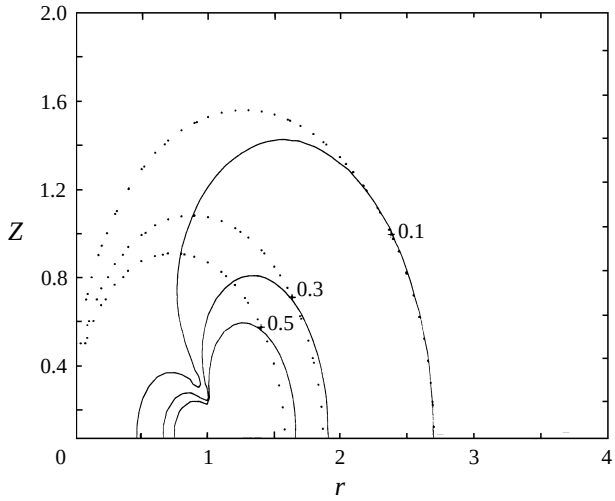

FIGURE 12. Horizontal strain field in (r, z) for point (dots) and circular-core (lines) vortices. The core thickness is 0.16, as in the CD solutions with $n = 25$.

in the form

$$\frac{\lambda^2 - 1}{\lambda^2} = \frac{\gamma(R,\ Z)}{\omega^{(i)}(\lambda) - \omega'(\lambda, R, Z)}, \tag{41}$$

where the right-hand side is the ratio of the strain rate (31) and the difference between the self-rotation rate (28) and the combination of mutual and local rotation rates (32). In the EM model, the strain rate is calculated as the far field of a point vortex while the mutual rotation rate includes a correction due to finite size of the vortex core. However, isolines of the strain field for a thin-core vortex deviate significantly from those for a point vortex, as shown in figure 12 for a circular core shape. In particular, the strain field for a finite-core vortex (as it is calculated in CD) is smaller in the vicinity of the upper boundary in figure 8, and this allows weakly deformed evolutions to occur at smaller Z values in CD than in EM.

7. Discussion

We have investigated the three-dimensional interaction of a close pair of like-sign vortices using two differently singularized models of the quasi-geostrophic equations (QG). We first derived and analysed an analytically tractable conservative (Hamiltonian), elliptical-moment (EM) model for thin-core vortices, which captures the strong elongation of vortex cores in response to horizontal straining, and we interpret this as an early evolutionary stage towards merger and alignment. This interpretation is strengthened by comparison with weakly dissipative numerical solutions of a thin contour-dynamics (CD) model, which both have a similar regime boundary to EM separating weakly and strongly deformed solutions and can reliably be followed further in the complexity of their deformations along the path towards merger and alignment.

Our principal conclusions are the following:

(i) The merger interaction of two vortices at the same vertical level is qualitatively similar to the that of two-dimensional vortices, as described by Melander *et al.* (1988). Stable co-rotating stationary states exist for sufficiently well separated vortices

but not for close ones, and initially close circular vortices exhibit strong elongation and decreasing horizontal separation (as required by conservation of total angular momentum).

(ii) For vertically separated vortices, there is a critical value of their vertical separation, $Z = Z_{cr}$, above which a stable stationary state exists always with moderate horizontal aspect ratio λ. In this regime all initially circular vortices with finite horizontal separation, $R \neq 0$, display a weak oscillation in λ while co-rotating.

(iii) For $0 < Z < Z_{cr}$, the interaction depends on σ (related to the normalized angular momentum of the vortex pair by $T/2JQ = \sigma^2 + 2$; see (23) and (A 47). For $\sigma < \sigma_C(Z) < \sigma_{cr}(Z)$, the only stationary state has moderate λ which approaches its minimum value $\lambda = 1$ when $\sigma \to 0$ for exactly aligned vortices. For $\sigma_C(Z) < \sigma < \sigma_{cr}(Z)$, the one stationary state has large λ and initially circular vortices exhibit strong core deformation and decreasing horizontal separation R through non-conservative filamentation or splitting. For $\sigma_{cr}(Z) < \sigma$, there are two stable stationary states, only one of which has weak core deformations. When there exists a weakly deformed stationary state, initially circular vortices display a weak oscillation in λ while co-rotating.

(iv) Both the EM and CD models show qualitatively similar regime boundaries as described above. In particular, there is a fairly close correspondence between the occurrence of strong core elongation in the EM solutions and significant filamentation and splitting in the CD solutions. The greatest inaccuracy of the EM model occurs in the approximation for the strain field for intermediate vertical separation distances between vortices, Z.

This paper takes some steps towards a theoretical understanding of the three-dimensional merger and alignment processes in a rotating stratified fluid. For reasons of mathematical simplicity, we have considered only the symmetric interaction of two vertically offset vortices with a thin core of uniform potential vorticity. We have found that the mutual strain field among the vortices cannot be balanced by co-rotation in a weakly elongated stationary state for a certain class of neighbouring, but substantially non-aligned, vortex configurations, and that such configurations will rapidly evolve towards a more aligned configuration through significantly non-conservative reorganizations of the potential vorticity field. Further investigation is required to test the aptness of these conclusions for non-singular vortices with finite core thickness; however, preliminary solutions indicate they are qualitatively apt, and we hope to report further on this in the future.

The stationary states and evolutionary tendencies shown here indicate that like-sign close vortices are usually likely to merge or align. This is consistent with the potential-vorticity amalgamation events seen in freely evolving geostrophic turbulence (McWilliams *et al.* 1994). A minor discrepancy, perhaps, is that a pair of vertically separated nearly aligned vortices in the models analysed here have no further tendency towards the complete alignment which seems to be approached in the turbulent solutions; we hypothesize that the latter requires an additional strain field (e.g. due to the moving remote vortices in turbulence) beyond that which occurs during a pair interaction.

We can also speculate that the alignment process is relevant to a wider range of flow structures than just the vortices investigated here. It allows for the growth of vertical correlation between potential vorticity patches located at different vertical levels, even in the absence of an advective or diffusive mechanism to vertically transport the potential vorticity, as in QG. This process, therefore, may be an important cause of the large vertical correlations commonly observed for temperature, velocity, etc.

This research was sponsored by of the National Science Foundation and the University of California through their support of NCAR and IGPP.

Appendix. The elliptic-moment model for thin-core vortices

A.1 *The evolution equations*

For thin-core vortices we reduce (12) to

$$(\dot{X}_k, \dot{Y}_k) = \sum_{m=0}^{\infty} \sum_{l=0}^{m} \frac{J_k^{(l,m-l,0)}}{l!(m-l)!} \partial_x^l \partial_y^{(m-l)} \boldsymbol{U}_k|_{\boldsymbol{R}_k}, \tag{A 1}$$

By omitting the third and higher horizontal moments in (14) and (A 1), we obtain truncated evolution equations similar to the second-order two-dimensional moment model considered by Melander *et al.* (1986):

$$J_k^{(0,0,0)} = 1, \tag{A 2}$$

$$\begin{pmatrix} \dot{X}_k \\ \dot{Y}_k \end{pmatrix} = [1 + \tfrac{1}{2}(J_k^{(2,0,0)}\partial_x^2 + 2J_k^{(1,1,0)}\partial_x\partial_y + J_k^{(0,2,0)}\partial_y^2)]\,\boldsymbol{U}_k|_{\boldsymbol{R}_k}, \tag{A 3}$$

$$\dot{J}_k^{(2,0,0)} = \dot{J}_{*k}^{(2,0,0)} + 2[J_k^{(1,1,0)}\partial_y U_k + J_k^{(2,0,0)}\partial_x U_k]_{\boldsymbol{R}_k}, \tag{A 4}$$

$$\dot{J}_k^{(0,2,0)} = \dot{J}_{*k}^{(0,2,0)} + 2[J_k^{(1,1,0)}\partial_x V_k + J_k^{(0,2,0)}\partial_y V_k]_{\boldsymbol{R}_k}, \tag{A 5}$$

$$\dot{J}_k^{(1,1,0)} = \dot{J}_{*k}^{(1,1,0)} + [J_k^{(2,0,0)}\partial_x V_k + J_k^{(0,2,0)}\partial_y U_k]_{\boldsymbol{R}_k}. \tag{A 6}$$

Here the far-field velocity and its derivatives $\partial_x^l \partial_y^m \boldsymbol{U}_k|_{\boldsymbol{R}_k}$ are calculated at the centroid $\boldsymbol{R}_k = (X_k, Y_k, Z_k)$.

For an elliptical vortex the volume conservation (A 2) follows from the system (A 4)–(A 6) in the same manner as shown for two dimensions by Melander *et al.* (1986):

$$J_k^{(2,0,0)} J_k^{(0,2,0)} - J_k^{(1,1,0)} J_k^{(1,1,0)} = J_k^2 = \text{const}, \tag{A 7}$$

where $J_k = \text{const}$ is the horizontal moment of inertia for a circular core.

Further we introduce the following non-dimensional notation for the second moments:

$$J_k^{(2,0,0)} = J_k \frac{\nu_k + \zeta_k}{2}, \quad J_k^{(0,2,0)} = J_k \frac{\nu_k - \zeta_k}{2}, \quad J_k^{(1,1,0)} = J_k \frac{\eta_k}{2}, \tag{A 8}$$

where ν_k and ζ_k are the sum and difference of the main moments. Correspondingly, (A 7) takes the form

$$\nu_k^2 - \zeta_k^2 - \eta_k^2 = 4. \tag{A 9}$$

The second horizontal moments define an equivalent ellipse with horizontal semi-axes a_k, b_k and the angle ϕ between the major axis and x-direction, so that

$$\nu_k = \lambda_k + \frac{1}{\lambda_k}, \quad \zeta_k = \left(\lambda_k - \frac{1}{\lambda_k}\right)\cos 2\phi_k, \quad \eta_k = \left(\lambda_k - \frac{1}{\lambda_k}\right)\sin 2\phi_k \tag{A 10}$$

where $\lambda_k = a_k/b_k$ is the aspect ratio. We will refer to this level of truncation as the elliptical-moment model (EM).

Thus, in the EM model the evolution of every thin vortex is also described by four parameters as for two-dimensional vortices: the centroid coordinates (X_k, Y_k), the aspect ratio λ_k and the angle ϕ_k.

A.2. *The far-field expansion*

The far-field velocity according to (9) is represented by the sum of the external flow and normalized velocity $\boldsymbol{U}_{k\alpha} = (-\partial_y \Psi_{k\alpha},\ \partial_x \Psi_{k\alpha})$, where the normalized streamfunction of the far field is

$$\Psi_{k\alpha}(x,\ y,\ Z_k) = \frac{1}{W_\alpha}\int_{W_\alpha} G(\rho_\alpha, Z_k, Z_\alpha)\mathrm{d}x'\mathrm{d}y'\mathrm{d}z'. \tag{A 11}$$

In stratified fluid for constant $N = 1$ and unbounded domain, the Green's function G depends only on the three-dimensional distance $\mathscr{R}$,

$$G = -\frac{1}{4\pi\mathscr{R}}, \quad \mathscr{R}^2 \equiv 2\rho_\alpha + (Z_k - Z_\alpha)^2. \tag{A 12}$$

For remote vortices we represent $\mathscr{R}^2$ in the form

$$\mathscr{R}^2 = \mathscr{R}_\alpha^2 - 2r_\alpha r' \cos(\theta_\alpha - \theta') + r'^2, \tag{A 13}$$

where

$$\mathscr{R}_\alpha^2 = r_\alpha^2 + (Z_k - Z_\alpha)^2, \quad \begin{pmatrix} x - X_\alpha \\ y - Y_\alpha \end{pmatrix} = r_\alpha \begin{pmatrix} \cos\theta_\alpha \\ \sin\theta_\alpha \end{pmatrix}, \quad \begin{pmatrix} x' \\ y' \end{pmatrix} = r' \begin{pmatrix} \cos\theta' \\ \sin\theta' \end{pmatrix}. \tag{A 14}$$

Assuming $|\mathscr{R}^2 - \mathscr{R}_\alpha^2| \ll \mathscr{R}_\alpha^2$, i.e. all vortex cores are well separated, either horizontally or vertically, we expand G as follows:

$$G(\mathscr{R}) = G(\mathscr{R}_\alpha) + \hat{G}(\mathscr{R}_\alpha)[\tfrac{1}{2}r'^2 - r_\alpha r' \cos(\theta_\alpha - \theta')] - \Upsilon_\alpha r'^2 \cos^2(\theta_\alpha - \theta') + \ldots. \tag{A 15}$$

Here we introduce

$$\hat{G}(\mathscr{R}_\alpha) \equiv \frac{\partial G}{\partial \rho} = \frac{1}{4\pi\mathscr{R}_\alpha^3}, \quad \Upsilon_\alpha \equiv -\rho_\alpha \frac{\partial \hat{G}}{\partial \rho} = \frac{3r_\alpha^2}{8\pi\mathscr{R}_\alpha^5}. \tag{A 16}$$

As we shall see below, $\hat{G}$ and Υ characterize the angular velocity and the strain rate induced by the point geostrophic vortex with infinitesimal core size.

Inserting (A 15) into (A 11), we obtain an approximate expression

$$\Psi_{k\alpha} \approx G(\mathscr{R}_\alpha) + \frac{J_\alpha}{2}\Psi'_{k\alpha}. \tag{A 17}$$

The first term in (A 17) describes the far field of the point vortex, while the other term, being proportional to J_α, represent effects of finite horizontal size of the vortex core:

$$\begin{aligned} \Psi'_{k\alpha} &= \Omega_\alpha v_\alpha - \Upsilon_\alpha(\zeta_\alpha \cos 2\theta_\alpha + \eta_\alpha \sin 2\theta_\alpha) \\ &= \Omega_\alpha\left(\lambda_\alpha + \frac{1}{\lambda_\alpha}\right) - \Upsilon_\alpha\left(\lambda_\alpha - \frac{1}{\lambda_\alpha}\right)\cos(2\theta_\alpha - 2\phi_\alpha), \end{aligned} \tag{A 18}$$

where Ω_α characterizes the induced rotational frequency

$$\Omega_\alpha \equiv \hat{G}(\mathscr{R}_\alpha) - \Upsilon_\alpha = \frac{2(z - Z_\alpha)^2 - r_\alpha^2}{8\pi\mathscr{R}_\alpha^5}, \tag{A 19}$$

which becomes negative for $r_\alpha > \sqrt{2}|z - Z_\alpha|$.

In this expansion we keep the general notation for $G, \hat{G}, \Upsilon, \Omega$ for a comparison with the two-dimensional flow when G does not depend on z (§ A.6).

A.3. *Centroid motion*

The centroid motion according to (A 3) is described by the sum of the normalized far-field velocity calculated by differentiating (A 17)

$$\boldsymbol{U}_{k\alpha} = \frac{\partial \Psi_{k\alpha}}{\partial r_\alpha}\begin{pmatrix}-\sin\theta_\alpha\\ \cos\theta_\alpha\end{pmatrix} - \frac{1}{r_\alpha}\frac{\partial \Psi_{k\alpha}}{\partial \theta_\alpha}\begin{pmatrix}\cos\theta_\alpha\\ \sin\theta_\alpha\end{pmatrix} \tag{A 20}$$

and the second derivatives of $\boldsymbol{U}_{k\alpha}$ at the centroid, which are calculated using the point-vortex velocity

$$\boldsymbol{U}^0_{k\alpha} = r_\alpha \hat{G}(\mathscr{R}_\alpha)\begin{pmatrix}-\sin\theta_\alpha\\ \cos\theta_\alpha\end{pmatrix}. \tag{A 21}$$

To calculate the far-field velocity we rewrite the correction of the normalized far-field streamfunction (A 17) in the form

$$\Psi'_{k\alpha} = \tfrac{1}{2}\Omega_\alpha(v_\alpha + \zeta_\alpha\cos 2\theta_\alpha + \eta_\alpha \sin 2\theta_\alpha) - \tfrac{1}{2}\hat{G}(R_\alpha)(\zeta_\alpha\cos 2\theta_\alpha + \eta_\alpha\sin 2\theta_\alpha). \tag{A 22}$$

Inserting (A 22) into (A 20), we obtain an approximate expression for a correction of the normalized velocity induced by the αth vortex within the kth vortex,

$$\boldsymbol{U}'_{k\alpha} = \frac{r_\alpha}{2}\frac{\partial \Omega_\alpha}{\partial \rho_\alpha}(v_\alpha + \zeta_\alpha\cos 2\theta_\alpha + \eta_\alpha\sin 2\theta_\alpha)\begin{pmatrix}-\sin\theta_\alpha\\ \cos\theta_\alpha\end{pmatrix} + \frac{\Upsilon_\alpha}{r_\alpha}\begin{pmatrix}-\zeta_\alpha\sin 3\theta_\alpha + \eta_\alpha\cos 3\theta_\alpha\\ \zeta_\alpha\cos 3\theta_\alpha + \eta_\alpha\sin 3\theta_\alpha\end{pmatrix}. \tag{A 23}$$

The second derivatives of $\boldsymbol{U}_k$ in (A 3) at the centroid are calculated using the point vortex velocity (A 21)

$$\left[\frac{v_k}{4}(\partial_x^2+\partial_y^2) + \frac{\zeta_k}{4}(\partial_x^2-\partial_y^2) + \frac{\eta_k}{2}\partial_x\partial_y\right]\boldsymbol{U}^0_{k\alpha} = \frac{r_{k\alpha}}{2}\frac{\partial\Omega_\alpha}{\partial\rho}(v_k + \zeta_k\cos 2\theta_{k\alpha} + \eta_k\sin 2\theta_{k\alpha})\begin{pmatrix}-\sin\theta_{k\alpha}\\ \cos\theta_{k\alpha}\end{pmatrix} + \frac{\Upsilon_{k\alpha}}{r_{k\alpha}}\begin{pmatrix}-\zeta_k\sin 3\theta_{k\alpha} + \eta_k\cos 3\theta_{k\alpha}\\ \zeta_k\cos 3\theta_{k\alpha} + \eta_k\sin 3\theta_{k\alpha}\end{pmatrix}. \tag{A 24}$$

Thus, summing (A 21), (A 23), and (A 24), for the centroid motion we obtain

$$\begin{pmatrix}\dot{X}_k\\ \dot{Y}_k\end{pmatrix} = \sum_{\alpha\neq k}^{M} Q_\alpha[(1 + J_\alpha B_\alpha + J_k B_k)\boldsymbol{U}^0_{k\alpha} + \frac{\Upsilon_{k\alpha}}{R_{k\alpha}}(J_\alpha \boldsymbol{V}_\alpha + J_k \boldsymbol{V}_k)], \tag{A 25}$$

where $R^2_{k\alpha} = (X_\alpha - X_k)^2 + (Y_\alpha - Y_k)^2$ while B_k and $\boldsymbol{V}_k$ are expressed as follows

$$B_\alpha = \frac{1}{2\hat{G}}\frac{\partial\Omega}{\partial\rho}\left[\lambda_\alpha + \frac{1}{\lambda_\alpha} + \left(\lambda_\alpha - \frac{1}{\lambda_\alpha}\right)\cos(2\theta_{k\alpha} - 2\phi_\alpha)\right], \tag{A 26}$$

$$\boldsymbol{V}_\alpha = \left(\lambda_\alpha - \frac{1}{\lambda_\alpha}\right)\begin{pmatrix}-\sin(3\theta_{k\alpha} - 2\phi_\alpha)\\ \cos(3\theta_{k\alpha} - 2\phi_\alpha)\end{pmatrix}. \tag{A 27}$$

Inserting expressions (A 16) and (A 19) into (A 26)–(A 27), finally for the centroid

motion of vertically offset geostrophic vortices we obtain

$$\begin{pmatrix}\dot{X}_k\\ \dot{Y}_k\end{pmatrix}=\sum_{\alpha\neq k}^{M}\frac{Q_\alpha r_{k\alpha}}{4\pi R_{k\alpha}^3}\begin{pmatrix}-\sin\theta_{k\alpha}\\ \cos\theta_{k\alpha}\end{pmatrix}$$
$$+\sum_{\alpha\neq k}^{M}\frac{3Q_\alpha r_{k\alpha}}{16\pi R_{k\alpha}^7}[r_{k\alpha}^2-4(Z_k-Z_\alpha)^2]\left\{A_\alpha\left(\lambda_\alpha+\frac{1}{\lambda_\alpha}\right)+A_k\left(\lambda_k+\frac{1}{\lambda_k}\right)\right.$$
$$\left.+A_\alpha\left(\lambda_\alpha-\frac{1}{\lambda_\alpha}\right)\cos(2\theta_{k\alpha}-2\phi_\alpha)+A_k\left(\lambda_k-\frac{1}{\lambda_k}\right)\cos(2\theta_{k\alpha}-2\phi_k)\right\}\begin{pmatrix}-\sin\theta_{k\alpha}\\ \cos\theta_{k\alpha}\end{pmatrix}$$
$$+\sum_{\alpha\neq k}^{M}\frac{3Q_\alpha r_{k\alpha}}{8\pi R_{k\alpha}^5}\left[A_\alpha\left(\lambda_\alpha-\frac{1}{\lambda_\alpha}\right)\begin{pmatrix}-\sin(3\theta_{k\alpha}-2\phi_\alpha)\\ \cos(3\theta_{k\alpha}-2\phi_\alpha)\end{pmatrix}+A_k\left(\lambda_k-\frac{1}{\lambda_k}\right)\begin{pmatrix}-\sin(3\theta_{k\alpha}-2\phi_k)\\ \cos(3\theta_{k\alpha}-\phi_k)\end{pmatrix}\right]. \tag{A 28}$$

A.4. *Core rotation and deformation*

To describe the deformation of the core we use representations of the horizontal moments $J_k^{(2,0,0)}$ and $J_k^{(0,2,0)}$ in terms of their sum and difference following (A 8), so that the evolution equations (A 4)–(A 6) become

$$\dot{v}_k=\Gamma_1\eta_k+\Gamma_2\zeta_k,\quad \dot{\zeta}_k=-\hat{\Omega}\eta_k+\Gamma_2 v_k,\quad \dot{\eta}_k=\hat{\Omega}\zeta_k+\Gamma_1 v_k, \tag{A 29}$$

where $\hat{\Omega}$ is defined by the self-interaction rotational frequency $\dot{\phi}^{(i)}$ and the far-field vorticity at the centre of the vortex

$$\hat{\Omega}=2\dot{\phi}^{(i)}+(\partial_x V_k)|_{\boldsymbol{R}_k}-(\partial_y U_k)|_{\boldsymbol{R}_k}, \tag{A 30}$$

while Γ_1 and Γ_2 describe the deformation of the vortex induced by remote vortices

$$\Gamma_1=(\partial_x V_k)|_{\boldsymbol{R}_k}+(\partial_y U_k)|_{\boldsymbol{R}_k},\quad \Gamma_2=(\partial_x U_k)|_{\boldsymbol{R}_k}-(\partial_y V_k)|_{\boldsymbol{R}_k}. \tag{A 31}$$

In terms of the horizontal aspect ratio λ_k and the angle ϕ_k, using (A 9) we rewrite (A 29) in the form

$$\frac{\dot{\lambda}_k}{\lambda_k}=\Gamma_1\sin 2\phi_k+\Gamma_2\cos 2\phi_k, \tag{A 32}$$

$$2\dot{\phi}_k=\hat{\Omega}+\frac{\lambda_k^2+1}{\lambda_k-1}(\Gamma_1\cos 2\phi_k-\Gamma_2\sin 2\phi_k). \tag{A 33}$$

The shear and strain produced by the αth vortex on the kth vortex in (A 29) are described by the normalized point-vortex velocity (A 21)

$$\partial_x U_{k\alpha}=-\partial_y V_{k\alpha}=\Upsilon_{k\alpha}\sin 2\theta_{k\alpha}, \tag{A 34}$$

$$\partial_x V_{k\alpha}=\Omega_{k\alpha}-\Upsilon_{k\alpha}\cos 2\theta_{k\alpha},\quad \partial_y U_{k\alpha}=-\Omega_{k\alpha}-\Upsilon_{k\alpha}\cos 2\theta_{k\alpha}, \tag{A 35}$$

$$\partial_z U_{k\alpha}=-\frac{2(Z_k-Z_\alpha)}{r_{k\alpha}}\Upsilon_{k\alpha}\sin\theta_{k\alpha},\quad \partial_z V_{k\alpha}=\frac{2(Z_k-Z_\alpha)}{r_{k\alpha}}\Upsilon_{k\alpha}\cos\theta_{k\alpha}, \tag{A 36}$$

where the strain rate $\Upsilon_{k\alpha}$ and the induced rotational frequency $\Omega_{k\alpha}$ are defined by (A 16) and (A 19), correspondingly.

Inserting (A 34)–(A 36) into (A 30)–(A 31), we obtain

$$\hat{\Omega} = \dot{\phi}^{(i)} + 2\sum_{\alpha\neq k}^{M} Q_\alpha \Omega_{k\alpha}, \tag{A 37}$$

$$\Gamma_1 = 2\sum_{\alpha\neq k}^{M} Q_\alpha \Upsilon_{k\alpha}\cos 2\theta_{k\alpha}, \quad \Gamma_2 = 2\sum_{\alpha\neq k}^{M} Q_\alpha \Upsilon_{k\alpha}\sin 2\theta_{k\alpha}. \tag{A 38}$$

Thus, using (A 37)–(A 38) in (A 32)–(A 33), we obtain

$$\dot{\lambda}_k = 2\lambda_k \sum_{\alpha\neq k}^{M} Q_\alpha \Upsilon_{k\alpha}\sin(2\theta_{k\alpha} - 2\phi_k), \tag{A 39}$$

$$\dot{\phi}_k = \dot{\phi}_k^{(i)} + \sum_{\alpha\neq k}^{M} Q_\alpha \left(\Omega_{k\alpha} - \frac{\lambda_k^2+1}{\lambda_k^2-1}\Upsilon_{k\alpha}\cos(2\theta_{k\alpha} - 2\phi_k)\right), \tag{A 40}$$

For three-dimensional geostrophic vortices at the same level $Z_k = Z_\alpha$ and $R_{k\alpha} = \mathscr{R}_{k\alpha}$. We see from (A 16) that ($\Upsilon_{k\alpha} = 3\hat{G}_{k\alpha}/2 = 3/8\pi R_{k\alpha}^3$), and according to (A 19), the induced rotational frequency $\Omega_{k\alpha} = -\hat{G}_{k\alpha}/2$ is negative. Thus, (A 39)–(A 40) correspond to formula (22) in the paper by Zhmur & Shchepetkin (1992) describing the internal frequency of rotation of an ellipsoidal core around the vertical axis as

$$\dot{\phi}^{(i)} = q\kappa_e\omega_e, \quad \omega_e(\lambda,\ \kappa_e) = \frac{1}{2}\int_0^\infty \frac{\xi\,\mathrm{d}\xi}{[(\lambda+\xi)(\lambda^{-1}+\xi)]^{3/2}(\kappa_e^2+\xi)^{1/2}}, \tag{A 41}$$

where $\kappa_e = c_e/(a_e b_e)^{1/2}$ is dimensionless thickness of the ellipsoidal core with the semi-axes a_e, b_e, c_e. In the limit of a thin core ($\kappa_e^2 \ll 1$), ω_e is expressed through complete elliptic integrals of the first kind K and the second kind E

$$\omega_e(\lambda,\ 0) = \int_0^\infty \frac{\xi^{1/2}\mathrm{d}\xi}{[(\lambda+\xi)(\lambda^{-1}+\xi)]^{3/2}} = \frac{(1-\epsilon^2)^{3/4}}{\epsilon^2}[2\mathrm{D}(\epsilon) - \mathrm{K}(\epsilon)], \tag{A 42}$$

where $\mathrm{D} = (\mathrm{K}-\mathrm{E})/\epsilon^2$ and $\epsilon^2 = 1 - 1/\lambda^2$.

The set of equations (A 25)–(A 27), (A 39)–(A 42) describes the evolution of vertically offset elliptical geostrophic vortices.

A.5 *Conserved quantities*

Like the two-dimensional Euler equations, the three-dimensional QG equations (1)–(3) are known to conserve the following: any analytic functional of potential vorticity $\Pi(q)$,

$$\frac{\mathrm{d}}{\mathrm{d}t}\int \Pi(q)\mathrm{d}x\,\mathrm{d}y\,\mathrm{d}z = 0; \tag{A 43}$$

global centroid,

$$\frac{\mathrm{d}}{\mathrm{d}t}\int q\begin{pmatrix}x\\y\\z\end{pmatrix}\mathrm{d}x\,\mathrm{d}y\,\mathrm{d}z = \int q\begin{pmatrix}-\partial_y p\\ \partial_x p\\ 0\end{pmatrix}\mathrm{d}x\,\mathrm{d}y\,\mathrm{d}z = 0; \tag{A 44}$$

angular momentum,

$$\frac{\mathrm{d}T}{\mathrm{d}t} \equiv \frac{\mathrm{d}}{\mathrm{d}t}\int q(x^2+y^2)\mathrm{d}x\,\mathrm{d}y\,\mathrm{d}z = 2\int q(-x\partial_y p + y\partial_x p)\mathrm{d}x\,\mathrm{d}y\,\mathrm{d}z = 0; \tag{A 45}$$

and sum of kinetic and potential energy,

$$\frac{\mathrm{d}H}{\mathrm{d}t} \equiv \frac{1}{2}\frac{\mathrm{d}}{\mathrm{d}t}\int [(\partial_x p)^2 + (\partial_y p)^2 + \frac{1}{N^2}(\partial_z p)^2]\mathrm{d}x\,\mathrm{d}y\,\mathrm{d}z = 0. \tag{A 46}$$

For vortices with thin compact cores of uniform potential vorticity, (A 43) corresponds to area conservation at the horizontal section. Both global centroid velocity (A 44) and the rate of change of angular momentum (A 45) vanish because the dynamic pressure (4) is an integral over a kernel G with odd horizontal symmetry (without the external flow $\overline{P} = 0$). The angular momentum is expressed through the second moments:

$$T = \int q(x^2 + y^2)\mathrm{d}x\,\mathrm{d}y\,\mathrm{d}z = \sum_{k=1}^{M} q_k \int_{W_k} [X_k^2 + Y_k^2 + 2x'X_k + y'Y_k + x'^2 + y'^2]\mathrm{d}x'\mathrm{d}y'\mathrm{d}z'$$

$$= \sum_{k=1}^{M} Q_k \left[X_k^2 + Y_k^2 + J_k\left(\lambda_k + \frac{1}{\lambda_k}\right)\right]. \tag{A 47}$$

Here the terms proportional to $X_k^2 + Y_k^2$ are the same as in the point-vortex model while another term proportional to J_k is the correction due to finite horizontal size of the vortex core.

Integrating (A 46) by parts and assuming the dynamic pressure tends to zero at infinity, we express geostrophic energy in the form

$$H \equiv -\frac{1}{2}\int qp\ \mathrm{d}x\,\mathrm{d}y\,\mathrm{d}z = H_C + H_I + \sum_{k=1}^{M} H_k^{(i)}, \tag{A 48}$$

where $H_C + H_I$ is the interaction energy due to a far field $\boldsymbol{U}_k = (-\partial_y \Psi_k,\ \partial_x \Psi_k)$:

$$H_C + H_I = -\sum_{k=1}^{M} \frac{q_k}{2}\int_{W_k} \Psi_k\ \mathrm{d}x\,\mathrm{d}y\,\mathrm{d}z, \tag{A 49}$$

while the last term in (A 48) is the self-energy of a near field $\boldsymbol{U}_k = (-\partial_y \psi_k,\ \partial_x \psi_k)$:

$$H_k^{(i)} = -\frac{q_k}{2}\int_{W_k} \psi_k\ \mathrm{d}x\,\mathrm{d}y\,\mathrm{d}z. \tag{A 50}$$

Note, that the energy of localized three-dimensional geostrophic vortices in an unbounded domain is finite in contrast to two dimensions.

The interaction energy is obtained by expanding the far field and truncating after the second-order moments as in (A 13)–(A 18)

$$H_C + H_I = -\frac{Q_k}{2}\sum_{\alpha\neq k}^{M} Q_\alpha \int_{W_\alpha} \Psi_{k\alpha}\mathrm{d}x'\mathrm{d}y'\mathrm{d}z'$$

$$= -\frac{Q_k}{2}\sum_{\alpha\neq k}^{M} Q_\alpha \left\{1 + \frac{J_k}{4}[\nu_k(\partial_x^2 + \partial_y^2) + \zeta_k(\partial_x^2 - \partial_y^2) + \eta_k \partial_x\partial_y]\right\} \Psi_{k\alpha}|_{\boldsymbol{R}_k}, \tag{A 51}$$

where $\Psi_{k\alpha}$ is described by (A 17)–(A 18).

Thus, the interaction energy consists of H_C, defined only by the inter-centroidal

distances (and is identical with the interaction energy of M geostrophic point vortices)

$$H_C = -\sum_{k=1}^{M}\sum_{\alpha\neq k}^{M}\frac{Q_k Q_\alpha}{2}G(R_{k\alpha}), \tag{A 52}$$

and H_I which represents the second-order correction due to finite size of the core

$$H_I = -\sum_{k=1}^{M}\sum_{\alpha\neq k}^{M}\frac{Q_k Q_\alpha}{4}\Omega_{k\alpha}\left[J_k\left(\lambda_k+\frac{1}{\lambda_k}\right)+J_\alpha\left(\lambda_\alpha+\frac{1}{\lambda_\alpha}\right)\right]$$

$$+\sum_{k=1}^{M}\sum_{\alpha\neq k}^{M}\frac{Q_k Q_\alpha}{4}\Upsilon_{k\alpha}\left[J_k\left(\lambda_k-\frac{1}{\lambda_k}\right)\cos(2\theta_{k\alpha}-2\phi_k)+J_\alpha\left(\lambda_\alpha-\frac{1}{\lambda_\alpha}\right)\cos(2\theta_{k\alpha}-2\phi_\alpha)\right]. \tag{A 53}$$

The first part of H_I is defined by the induced rotational frequency Ω while the other parts of H_I are defined by the strain rate Υ. In two dimensions the first part of H_I vanishes because $\Omega = 0$, so that (A 52)–(A 53) correspond to expressions (28) in the paper by Melander *et al.* (1986).

From (A 52)–(A 53) in agreement with (A 25)–(A 27) we find

$$Q_k\dot{Y}_k = -\partial_{X_k}(H_C+H_I), \quad Q_k\dot{X}_k = \partial_{Y_k}(H_C+H_I) \tag{A 54}$$

(similar to the Hamiltonian form of the point-vortex model).

For the other variables in agreement with (A 39)–(A 40) we find

$$Q_k J_k(\lambda_k^2-1)\frac{\dot{\lambda}_k}{2\lambda_k^2} = \partial_{\phi_k}H_I, \tag{A 55}$$

$$Q_k J_k(\lambda_k^2-1)\frac{\dot{\phi}_k}{2\lambda_k^2} = -\partial_{\lambda_k}(H_I+H_k^{(i)}), \tag{A 56}$$

assuming that the self-energy of an elliptical vortex does not depend on its orientation, so that $\dot{\lambda}_k^{(i)} = 0$. The interaction energy and self-energy for geostrophic vortices with an ellipsoidal core have been calculated by Zhmur & Pankratov (1990):

$$H^{(i)} = \frac{q^2 W_e J_e \kappa_e}{2}h_e(\lambda,\kappa_e), \quad h_e = \int_0^\infty \frac{\mathrm{d}\xi}{[(\lambda+\xi)(\lambda^{-1}+\xi)(\kappa_e^2+\xi)]^{1/2}}. \tag{A 57}$$

In the limit of a thin ellipsoidal core when $\kappa_e \ll 1$, $h_e(\lambda,\ 0)$ is expressed through a complete elliptic integral of the first kind K (ϵ)

$$h_e = 2(1-\epsilon^2)^{1/4}\mathrm{K}(\epsilon), \quad \epsilon^2 = 1-\frac{b_e^2}{a_e^2}. \tag{A 58}$$

corresponding to the internal rotational frequency (A 42).

Thus, (A 54)–(A 57) yields the energy conservation for the EM model:

$$\frac{\mathrm{d}H}{\mathrm{d}t} = \sum_{k=1}^{M}[\dot{X}_k\partial_{X_k}H + \dot{Y}_k\partial_{Y_k}H + \dot{\lambda}_k\partial_{\lambda_k}H + \dot{\phi}_k\partial_{\phi_k}H] = 0. \tag{A 59}$$

A.6. *Comparison with two-dimensional vortex interactions*

It is useful to compare the 3D EM model with its 2D analogue when

$$G = \frac{1}{4\pi}\ln 2\rho = \frac{1}{2\pi}\ln r, \quad \hat{G} = \Upsilon = \frac{1}{4\pi\rho} = \frac{1}{2\pi r^2}, \quad \Omega = 0. \tag{A 60}$$

Thus, in the 2D limit from (A 26), we see that $B_\alpha = 0$ because of $\Omega_\alpha = 0$, and from (A 25)–(A 27) with (A 60), we obtain the formulae (67) in the paper by Melander *et al.*, (1986) if we represent total vorticity of the core as $Q_\alpha = \omega_\alpha A_\alpha$, assuming ω_α is the two-dimensional vorticity, $J_\alpha = A_\alpha/4\pi$, and A is the core area. Further, (A 39)–(A 40) correspond to equations (59)–(60) in the paper by Melander *et al.* (1986) with the self-induced rotation frequency

$$\dot{\phi}^{(i)} = \frac{q\lambda}{(1+\lambda)^2} \tag{A 61}$$

corresponding to well-known Kirchhoff's solution which describes exactly steady rotation of an elliptic vortex.

The problem of the interaction two identical vortices in the two-dimensional limit is described by (21)–(24) on substituting (A 60). In this case $Q = 4\pi qJ$, $\mu = 0$ and if we normalize the distance between vortices by $r_0 = (A/\pi)^{1/2} = 2J^{1/2}$ expressions (A 60) become

$$\hat{G} = \Upsilon = \frac{1}{2\pi(\sigma^2 + 2 - v)}. \tag{A 62}$$

Thus, (30)–(32) which describe the stationary states, can be written as

$$\sigma^2 = \lambda + \frac{1}{\lambda} - 2 + \frac{1}{2\omega^{(i)}}\left(1 + \frac{2\lambda^2}{\lambda^2 - 1} + F\right), \quad F = \frac{\lambda^2 - 1}{\lambda(\sigma^2 + 2) - \lambda^2 - 1} \tag{A 63}$$

with the normalized self-induced rotational frequency (A 61),

$$\omega^{(i)} = \frac{4\pi J\dot{\phi}^{(i)}}{Q} = \frac{\lambda}{(1+\lambda)^2}. \tag{A 64}$$

The system (A 63)–(A 64) corresponds to equation (28) in the paper by Melander *el al.* (1988). We see that (A 63) is a quadratic equation for σ^2, hence the angular momentum is explicitly expressed through the aspect ratio λ. The value of σ increases either when $\lambda \to 1$ or $\lambda \to \infty$. Thus, two solutions exist when σ exceeds its minimum value σ_{cr}. As shown by Melander *et al.* (1988), this pair of stable and non-stable stationary states corresponds to the centre and saddle points of H.

Note, that in two dimensions the term F in the right-hand side of (A 63) gives only a small correction because large σ is the basic assumption of the two-dimensional moment model. If we consider the minimum value of σ defined by the minimum of the right-hand side of (A 63) while neglecting F, we obtain $\sigma_{cr} \approx 2.96$ at $\lambda \approx 1.97$, which is quite close to the critical value $\sigma_{cr} = 3.08$ at $\lambda = 1.93$ obtained from (A 63) taking into account a correction term F.

A.7. *Thin-core and ellipsoidal vortices*

For the circular disk-shaped core of radius r_d with uniform thickness $2h_d$, the area of each horizontal section is the same, so that

$$W_d = 2h_d A_d, \quad J_d = \frac{2\pi h_d}{W_d}\int_0^{r_d} r^3 \mathrm{d}r = \frac{A_d}{4\pi}, \tag{A 65}$$

while for the circular ellipsoidal core of radius r_e with the vertical semi-axis c_e the thickness varies as $2c_e(1 - r^2/r_e^2)^{1/2}$, so that

$$W_e = \tfrac{4}{3}c_e A_e, \quad J_e = \frac{2\pi c_e}{W_e}\int_0^{r_e}\left(1 - \frac{r^2}{r_e^2}\right)^{1/2} r^3 \mathrm{d}r = \frac{A_e}{5\pi}. \tag{A 66}$$

Thus, for an equivalent ellipsoid with the same volume $W_e = W_d$ and the horizontal moment $J_e = J_d$, we have

$$\frac{c_e}{r_e} = \chi \frac{h_d}{r_d}, \quad \chi = \frac{12}{5\sqrt{5}}. \tag{A 67}$$

The self-induced rotational frequency for a thin elliptical vortex can be expressed in the form

$$\dot{\phi}_k^{(i)} = \frac{q_k h_k}{r_k} \omega_d(\lambda_k), \tag{A 68}$$

where

$$\omega_d(\lambda) = 2\left(\frac{\lambda}{\lambda^2 - 1}\right)^{3/2} \left(\frac{2}{\pi} \ln[\lambda + (\lambda^2 - 1)^{1/2}] + \frac{2}{\pi} \tan^{-1} \frac{1}{(\lambda^2 - 1)^{1/2}} - 1\right). \tag{A 69}$$

Note, that (A 69) is obtained using approximations of a thin and nearly elliptical vortex core when variations of the aspect ratio due to the self-interaction are small in contrast to exact expression (A 42) for a thin ellipsoidal core. However, actually the difference between (A 42) and (A 69) is small.

REFERENCES

Abrashkin, A. A. 1987 Toward a theory of interaction of two planar vortices in an ideal fluid. *Izv. Mech. Zhidk. Gaza* No 1, 62–68 (in Russian).

Carnevale, G. F., McWilliams, J. C., Pomeau, Y., Weiss, J. B. & Young, W. R. 1992 Rates, pathways, and end-states of nonlinear evolution in decaying two-dimensional turbulence: Scaling theory vs. selective decay. *Phys. Fluids* A **4**, 1314–1316.

Charney, J. G. 1971 Geostrophic turbulence. *J. Atmos. Sci.* **28**, 1087–1095.

Dritschel, D. G. 1995 A general theory for two-dimensional vortex interactions. *J. Fluid Mech.* **293**, 269-303.

Dritschel, D. G. & Saravanan, R. 1994 Three-dimensional quasi-geostrophic contour dynamics, with an application to stratospheric vortex dynamics. *Q. J. R. Met. Soc.* **120**, 1267–1297.

Dritschel, D. G. & Waugh, D. W. 1992 Quantification of the inelastic interaction of unequal vortices in two-dimensional vortex dynamics. *Phys. Fluids* A **4**, 1737–1744.

Gryanik, V. M. 1983 Dynamics of localized vortex perturbations - "vortex charges" in a baroclinic fluid. *Izv. Atmos. Oceanic. Phys.* **19**, 347–352.

Herring, J. R. 1980 Statistical theory of quasigeostrophic turbulence. *J. Atmos. Sci.* **37**, 969–977.

Kida, S. 1981 Motion of an elliptic vortex in a uniform shear flow. *J. Phys. Soc. Japan* **50**, 3517–3520.

McWilliams, J. C. 1984 The emergence of isolated coherent vortices in turbulent flow. *J. Fluid Mech.* **146**, 21–43.

McWilliams, J. C. 1989 Statistical properties of decaying geostrophic turbulence. *J. Fluid Mech.* **198**, 199–230.

McWilliams, J. C. 1990 The vortices of two-dimensional turbulence. *J. Fluid Mech.* **219**, 361–385.

McWilliams, J. C., Weiss, J. B. & Yavneh, I. 1994 Anisotropy and coherent vortex structures in planetary turbulence. *Science* **264**, 410–413.

Meacham, S. P., Pankratov, K. K., Shchepetkin, A. F. & Zhmur, V. V. 1994 The interaction of ellipsoidal vortices with background shear flows in a stratified fluid. *Dyn. Atmos. Oceans* **27**, 167–212.

Melander, M. V., Zabusky, N. J. & McWilliams, J. C. 1988 Symmetric vortex merger in two dimensions: causes and conditions. *J. Fluid Mech.* **195**, 303–340.

Melander, M. V., Zabusky, N. J. & Styczek, A. S. 1986 A moment model for vortex interactions of the two-dimensional Euler equations. Part 1. Computational validation of a Hamiltonian elliptical representation. *J. Fluid Mech.* **167**, 95–115.

Polvani, L. M. 1991 Two-layer geostrophic vortex dynamics. Part 2. Alignment and two-layer V-states. *J. Fluid Mech.* **225**, 241–270.

RHINES, P. B. 1977 The dynamics of unsteady currents. In *The Sea: Marine Modelling*, vol. 6 (ed E. D. Goldberg, I. N. McCane, J. J. O'Brien & J. H. Steele), pp. 189–318. Wiley.

RHINES, P. B. 1979 Geostrophic turbulence. *Ann. Rev. Fluid Mech.* **11**, 401–441.

SALMON, R. 1982 Geostrophic turbulence. In *Topics in Ocean Physics, LXXX Corso*, pp. 30–78. Soc. Italiana di Fisica, Bologna.

SUTYRIN, G. G. 1989 The structure of a monopolar baroclinic eddy. *Oceanology* **29**, 139–144.

VIERA, F. 1995 On the alignment and axisymmetrization of a vertically tilted geostrophic vortex. *J. Fluid Mech.* **289**, 29–50.

WEISS, J. B. & MCWILLIAMS, J. C. 1993 Temporal scaling behavior of decaying two- dimensional turbulence. *Phys. Fluids* A **5**, 608–621.

ZHMUR, V. V. & PANKRATOV, K. K. 1989 Dynamics of semi-ellipsoidal subsurface vortex in a uniform flow. *Oceanology* **29**, 150–154.

ZHMUR, V. V. & PANKRATOV, K. K. 1990 Long-range interaction of an ensemble of quasigeostrophic ellipsoidal vortices. Hamiltonian formulation. *Izv. Atmos. Ocean. Phys.* **26**, 972–981.

ZHMUR, V. V. & SHCHEPETKIN, A .F. 1991 Evolution of an ellipsoidal vortex in a stratified ocean in the f-plane approximation. *Izv. Atmos. Ocean. Phys.* **27**, 337-345.

ZHMUR, V. V. & SHCHEPETKIN, A. F. 1992 Interaction between two quasigeostrophic baroclinic vortices: tendency to come together and merge. *Izv. Atmos. Ocean. Phys.* **28**, 407-417.